Myo1c regulates lipid raft recycling to control cell spreading, migration and *Salmonella* invasion

Hemma Brandstaetter[1], John Kendrick-Jones[2] and Folma Buss[1,*]

[1]Cambridge Institute for Medical Research, University of Cambridge, Wellcome Trust/MRC Building, Hills Road, Cambridge CB2 0XY, UK
[2]MRC Laboratory of Molecular Biology, Hills Road, Cambridge CB2 2QH, UK
*Author for correspondence (fb1@mole.bio.cam.ac.uk)

Accepted: 13 December 2011
Journal of Cell Science 125, 1991–2003

doi: 10.1242/jcs.097212

Summary

A balance between endocytosis and membrane recycling regulates the composition and dynamics of the plasma membrane. Internalization and recycling of cholesterol- and sphingolipid-enriched lipid rafts is an actin-dependent process that is mediated by a specialized Arf6-dependent recycling pathway. Here, we identify myosin1c (Myo1c) as the first motor protein that drives the formation of recycling tubules emanating from the perinuclear recycling compartment. We demonstrate that the single-headed Myo1c is a lipid-raft-associated motor protein that is specifically involved in recycling of lipid-raft-associated glycosylphosphatidylinositol (GPI)-linked cargo proteins and their delivery to the cell surface. Whereas Myo1c overexpression increases the levels of these raft proteins at the cell surface, in cells depleted of Myo1c function through RNA interference or overexpression of a dominant-negative mutant, these tubular transport carriers of the recycling pathway are lost and GPI-linked raft markers are trapped in the perinuclear recycling compartment. Intriguingly, Myo1c only selectively promotes delivery of lipid raft membranes back to the cell surface and is not required for recycling of cargo, such as the transferrin receptor, which is mediated by parallel pathways. The profound defect in lipid raft trafficking in Myo1c-knockdown cells has a dramatic impact on cell spreading, cell migration and cholesterol-dependent *Salmonella* invasion; processes that require lipid raft transport to the cell surface to deliver signaling components and the extra membrane essential for cell surface expansion and remodeling. Thus, Myo1c plays a crucial role in the recycling of lipid raft membrane and proteins that regulate plasma membrane plasticity, cell motility and pathogen entry.

Key words: Myo1c, Lipid raft, Migration, *Salmonella*, Membrane recycling

Introduction

The plasma membrane of eukaryotic cells is in a constant state of equilibrium with internal cellular membranes through membrane uptake (endocytosis) and reinsertion (exocytosis/recycling) from intracellular pools. In some cell types, the total cell surface is renewed every 15 minutes through such cycles of endocytosis and exocytosis (Steinman et al., 1983). This dynamic remodeling of the plasma membrane is especially important for controlling the surface area as well as for regulating the protein and lipid composition of the cell surface, which is crucial for biological processes such as cell migration, cell spreading and pathogen invasion.

Proteins and lipids of the plasma membrane assemble into small dynamic subdomains that can be stabilized to form larger specialized microdomains (Simons and Gerl, 2010; Simons and Toomre, 2000). These sphingolipid- and cholesterol-enriched lipid microdomains (herein referred to as lipid rafts) attract protein components and compartmentalize cellular processes associated with cell signaling and membrane trafficking (Simons and Gerl, 2010). Furthermore, it has recently been shown that when a cell detaches from a surface, these lipid rafts are rapidly internalized as part of the process to reduce the area of the plasma membrane (del Pozo et al., 2004). After endocytosis these membranes and associated rafts are delivered in an actin- and microtubule-dependent pathway to a perinuclear recycling endosome, which acts as a membrane storage compartment (Balasubramanian et al., 2007; Gauthier et al., 2009). Integrin-mediated re-adhesion of the cell during cell spreading triggers lipid raft exit from the recycling endosomes and exocytosis of glycosylphosphatidylinositol (GPI)-anchored lipid raft markers (Balasubramanian et al., 2007; del Pozo et al., 2005; Gauthier et al., 2009). These specialized lipid rafts are transported to the plasma membrane in order to deliver the signaling components and the extra membrane required for cell surface expansion and remodeling that are essential for cell spreading. This process is known to involve the small GTPase Arf6 (Balasubramanian et al., 2010; Balasubramanian et al., 2007; Radhakrishna et al., 1999; Radhakrishna and Donaldson, 1997), but the motor proteins required to deliver these lipid raft membranes to the plasma membrane have not yet been identified.

Myosin motor proteins are known to regulate the dynamic organization of the plasma membrane by generating and maintaining an actin-dependent force on the cell surface and by transporting and fusing membrane vesicles with it. Myosins are a large superfamily of more than 20 classes that use the energy derived from ATP hydrolysis to interact and translocate along actin filaments (Foth et al., 2006). Myosins occur as monomeric or dimeric motors with a diverse range of cellular roles, such as transporters, anchors or in tension maintenance (Krendel and Mooseker, 2005). Myosin1c (Myo1c) is a monomeric class I myosin with a single N-terminal catalytic motor (head) domain, a regulatory neck region that contains three IQ-motifs for

Journal of Cell Science

calmodulin binding and a C-terminal tail, which directly associates, through a putative pleckstrin homology domain, with phosphatidylinositol 4,5-bisphosphate [Ptd(4,5)InsP_2] in lipid membranes (Hokanson et al., 2006; Hokanson and Ostap, 2006; McKenna and Ostap, 2009). Although no adaptor proteins linking Myo1c to cargo such as membrane vesicles have been identified, the GTPase RalA has been shown to bind in a Ca^{2+}-calmodulin-dependent manner to the Myo1c regulatory neck region (Chen et al., 2007).

Myo1c is expressed in most eukaryotic cells and it has been shown that it localizes to the actin-rich cell periphery and the plasma membrane (Bose et al., 2004; Ruppert et al., 1995; Wagner et al., 1992). Myo1c has been shown to fulfill distinct functions in a number of specialized cell types. For example, in the sensory hair cells of the inner ear, Myo1c is present in the stereocilia tips, where it controls the tension of the tip links that connect neighboring stereocilia and thereby functions as a motor for slow adaptation (Gillespie and Cyr, 2004). It also functions in the trafficking of epithelial Na^+ channels within cortical collecting duct cells (Wagner et al., 2005) and in the translocation of Neph1-containing signaling complexes to the podocyte plasma membrane (Arif et al., 2011). Furthermore, Myo1c has been implicated in insulin-stimulated glucose transporter 4 (GLUT4) trafficking and plasma membrane fusion in adipocytes through its interaction with RalA (Chen et al., 2007). Thus, Myo1c facilitates the correct targeting of many different cargoes to the plasma membrane in a number of highly specialized cell types. However, because Myo1c is ubiquitously expressed, it is expected to have a more universal function in cargo delivery and membrane trafficking.

The objective of this study was to characterize the precise cellular functions of Myo1c. We demonstrate that Myo1c is a lipid-raft-associated motor protein that is crucial for the cellular distribution and trafficking of cargo molecules associated with these specialized membrane microdomains. Myo1c colocalizes on recycling tubules enriched in GPI-anchored proteins and specifically stabilizes these structures emanating from the perinuclear recycling compartment. Depletion of Myo1c leads to a loss of lipid-raft-linked proteins from the plasma membrane, which suggests a role for Myo1c in the exocytosis of lipid raft membranes from a perinuclear recycling compartment. These results thus reveal a novel molecular function, crucial for cell spreading, migration and pathogen entry, by which Myo1c mediates lipid raft exocytosis to dynamic sites on the plasma membrane.

Results

Myo1c associates with lipid raft microdomains

Myo1c has been shown to bind Ptd(4,5)InsP_2 in vitro (Hokanson and Ostap, 2006), a phospholipid found in cholesterol- and sphingolipid-enriched lipid rafts in cells (Hope and Pike, 1996; Rozelle et al., 2000). To investigate whether Myo1c associates with lipid rafts, HeLa cells were transiently transfected with GFP–Myo1c and incubated with the lipid-binding B subunit of cholera toxin (CTB) labeled with Alexa Fluor 555. CTB is a widely used lipid raft marker that binds to the glycosphingolipid GM1 (Eidels et al., 1983). CTB labeling was performed at 4℃ so as to prevent its internalization and thus it exclusively labeled cell surface lipid raft microdomains. Confocal imaging demonstrated that GFP–Myo1c was enriched in regions of the plasma membrane containing the lipid raft marker CTB (Fig. 1A). Colocalization with CTB was also observed for immunostained endogenous Myo1c (Fig. 1B).

The presence of Myo1c in these lipid microdomains was confirmed using a second major class of lipid raft markers, namely those that specifically anchor to the outer leaflet of raft microdomains through the GPI lipid modification. A number of functionally diverse cell surface proteins, including the CD55 and CD59 receptors, are targeted to lipid rafts through their GPI domain (Brown and Rose, 1992; Foster et al., 2003; Sprenger et al., 2004). To visualize the cellular distribution of this class of raft markers, we created a probe encoding GFP fused to a peptide containing a GPI-modification site (GFP–GPI) (Legler et al., 2005). When HeLa cells were co-transfected with mCherry–Myo1c and GFP–GPI, extensive colocalization was observed not only in filopodial extensions at the plasma membrane but also in intracellular tubular and vesicular membranes (Fig. 1C; supplementary material Movie 1). Time-lapse video microscopy demonstrates that these Myo1c- and GFP–GPI-positive tubules and vesicles were highly dynamic in live cells (supplementary material Movie 1).

To confirm further the association of Myo1c with lipid rafts, we used a flotation assay exploiting the inability of non-ionic detergents, such as Triton X-100, to solubilize lipid rafts at 4℃, which thus remain buoyant in low-density sucrose. HeLa cells stably expressing GFP–Myo1c were incubated with CTB–HRP (horseradish peroxidase) to label cell surface rafts, then lysed with a buffer solution containing 1% Triton X-100 at 4℃ and fractionated by ultracentrifugation on a bottom-loaded 40–5% sucrose step gradient. SDS-PAGE of equal amounts of fractions 1–10 demonstrated that most proteins were present in fractions 8, 9 and 10, whereas raft markers were found in fractions 3, 4 and 5, highlighting the significant enrichment of lipid rafts by this fractionation method (Fig. 1D). Immunoblotting demonstrated that proteins such as actin, calnexin, tubulin and ezrin, typically not associated with lipid rafts, were present in these detergent-soluble fractions, whereas lipid raft markers such as placental alkaline phosphatase (PLAP), flotillin-1 and flotillin-2 partitioned into the detergent-resistant fractions 3, 4 and 5 (Fig. 1E). The presence of lipid rafts in these floating fractions was further confirmed by dot-blotting for CTB–HRP. Importantly, Myo1c was observed enriched in lipid raft fractions, as were small amounts of RalA, a known binding partner of Myo1c.

Absence of Myo1c redistributes lipid raft markers from the cell surface to intracellular membranes

Because we have shown that Myo1c is present in specialized lipid domains at the plasma membrane, we investigated whether this myosin regulates lipid raft trafficking and distribution, thus controlling the area and dynamics of the plasma membrane. Therefore, we tested the effect of siRNA-mediated knockdown of Myo1c on the localization of several lipid raft associated marker proteins such as GFP–GPI and CD59 or CD55, as well as caveolin-1 and flotillin-1 and -2, which represent members of two other well characterized classes of membrane-associated proteins that mark distinct types of lipid raft domains (Foster et al., 2003; Sprenger et al., 2004). To ablate *MYO1C* expression, HeLa cells were transfected with a smart pool of four combined siRNA oligonucleotides specific to *MYO1C* or with the same four specific oligonucleotides individually. After two transfections Myo1c knockdown was confirmed by immunoblotting (supplementary material Fig. S1A). In mock-transfected control

cells, the marker proteins GFP–GPI, CD59, CD55, caveolin-1 and flotillin-1 and -2 were present in small distinct patches at the plasma membrane and in a number of intracellular vesicles (Fig. 2A,B; supplementary material Fig. S2A, Fig. S3A,B). In Myo1c-depleted cells, however, a substantial proportion of these marker proteins was lost from the plasma membrane and accumulated on internal membranes (Fig. 2A,B; supplementary material Fig. S2A, Fig. S3A,B). In the knockdown cells, flotillin-1 and -2 redistributed into internal swollen vesicles that partly colocalized with the lysosomal marker LAMP1 (supplementary material Fig. S3B), whereas caveolin-1 and GPI-anchored marker proteins accumulated in the perinuclear region, where they were observed by confocal microscopy to colocalize in a tight juxtanuclear spot (supplementary material Fig. S4A).

The redistribution of lipid raft marker proteins following Myo1c knockdown by the smart pool siRNA was not due to off-target effects caused by the depletion of unrelated proteins, because Myo1c knockdown mediated by each individual siRNA oligonucleotides also triggered relocalization of caveolin-1 and flotilin-2 from the plasma membrane to internal membranes (supplementary material Fig. S1B). This specific phenotype was further verified by overexpressing a dominant-negative Myo1c variant (the 'rigor' mutant) in which the motor function is inhibited by a single point mutation (K111R) in the ATP-binding site (Aschenbrenner et al., 2004; Ruppel and Spudich, 1996; Toyoda et al., 2011). In cells expressing this non-functional Myo1c rigor mutant, caveolin-1 (Fig. 2C) and flotillin-2 (supplementary material Fig. S3C) were depleted from the plasma membrane and accumulated on intracellular membrane compartments. Thus, abolishing Myo1c activity either by siRNA-mediated knockdown or by expressing a dominant-negative Myo1c mutant leads to a redistribution of lipid raft marker proteins from the plasma membrane to the perinuclear region near the microtubule organizing centre (Fig. 2). This collapsed lipid-raft-enriched membrane compartment is distinct from the Golgi complex, as it shows very little overlap with the Golgi marker GM130 and the trans-Golgi network protein TGN46 (supplementary material Fig. S4B,C), but shows partial colocalization with Rab11, a marker for the common endocytic recycling compartment (Fig. 5B; supplementary material Fig. S5C,D).

Because the absence of functional Myo1c leads to loss of lipid-raft-associated marker proteins from the cell surface, we tested whether elevated expression of Myo1c increases the level of lipid rafts at the plasma membrane. HeLa cells were transiently transfected with GFP–Myo1c and cell surface lipid rafts were labeled with CTB–Alexa-Fluor-555 (Fig. 3A). In the population of untransfected cells, a modest level of surface CTB was observed in ~80% of cells (Fig. 3A, see the cells marked with an asterisk), whereas ~20% displayed more intense surface CTB staining. In the population expressing GFP–Myo1c (Fig. 3A, see the cells marked with arrowheads), however, the percentage of cells with an intense CTB staining more than doubled (from ~20% to ~50%). To confirm these observations, a HeLa cell

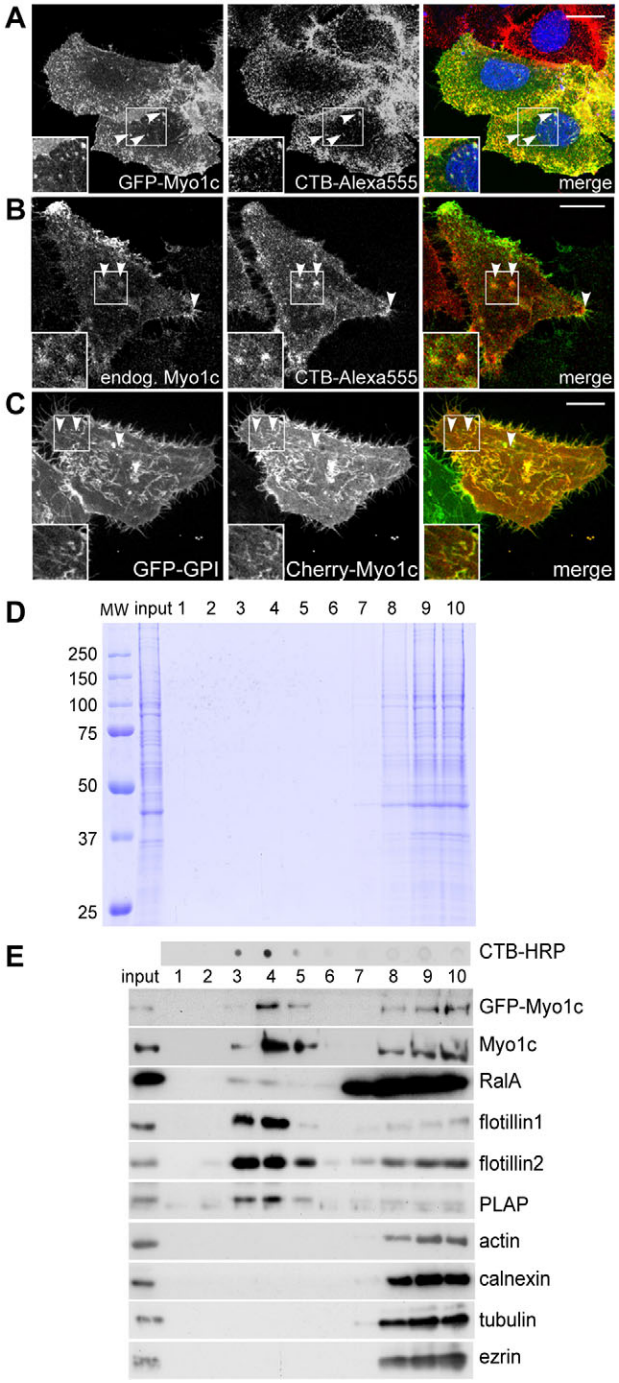

Fig. 1. Myo1c partitions into lipid rafts. Cell surface lipid rafts on HeLa cells transiently transfected with GFP–Myo1c (**A**) and non-transfected HeLa cells (**B**) were labeled with CTB–Alexa-Fluor-555 (CTB-Alexa555) and co-stained with antibodies against GFP (**A**) and endogenous Myo1c (**B**) for confocal microscopy. Cell nuclei are shown in blue in the merged image. Arrowheads highlight examples of colocalization of Myo1c with lipid rafts. (**C**) HeLa cells were co-transfected with GFP–GPI and mCherry–Myo1c, seeded onto fibronectin-coated coverslips and imaged using live-cell microscopy. The picture presented is a still image from the start point of a representative movie (supplementary material Movie 1). Arrowheads highlight the localization of Myo1c on lipid-raft-enriched tubules. Scale bars, 10 μm. The inserts are enlarged representations of the boxed regions. (**D**) HeLa cells stably expressing GFP–Myo1c were incubated with CTB–HRP on ice, lysed with cold 1% Triton X-100 and subjected to a sucrose gradient ultracentrifugation. The fractions were separated on SDS-PAGE and Coomassie stained. (**E**) Floating fractions (3–5) and detergent-soluble fractions (8–10) were identified based on the distribution of CTB–HRP by dot-blot analysis (top panel) and localization of marker proteins using western blotting with indicated antibodies (bottom panels).

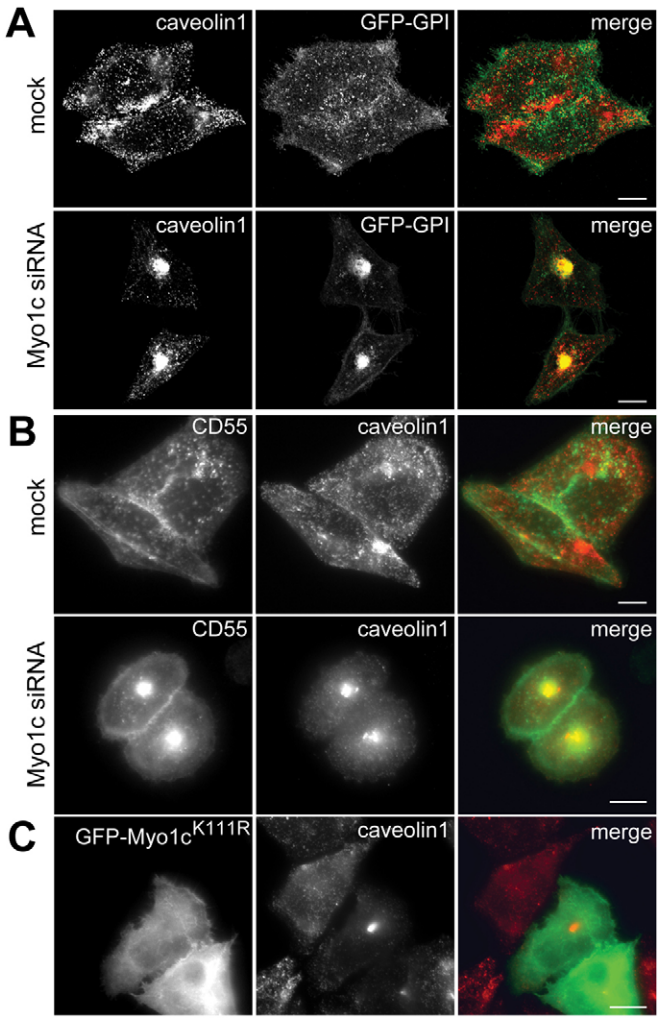

Fig. 2. Depletion of Myo1c causes accumulation of lipid rafts in the perinuclear region. (**A**) HeLa cells stably expressing GFP–GPI were either mock transfected or transfected with siRNA specific to *MYO1C* and labeled with antibodies against caveolin-1 and GFP for immunofluorescence microscopy. (**B**) Mock- or Myo1c-depleted HeLa cells were labeled with antibodies against the raft markers caveolin-1 and CD55. (**C**) HeLa cells transiently transfected with the dominant-negative GFP–Myo1c^{K111R} rigor mutant were labeled with antibodies against GFP and caveolin-1. Scale bars, 10 μm.

line stably expressing homogenous levels of GFP–Myo1c was created using FACS sorting (Fig. 3B). FACS analysis showed that the levels of cell-surface-bound CTB–Alexa-Fluor-647 increased in cells stably expressing GFP–Myo1c as compared with those in control cells (Fig. 3C).

Therefore, not only does the loss of Myo1c, but also its overexpression, affects the cellular distribution of proteins associated with lipid rafts. In cells without functional Myo1c, lipid raft markers accumulate on intracellular membranes, suggesting a role for Myo1c either in recycling or exocytosis of lipid-raft-enriched membranes from intracellular membrane compartments back to the cell surface.

Myo1c localizes on lipid-raft-enriched recycling tubules

RalA, a Myo1c-binding partner, has recently been shown to regulate lipid raft exocytosis from recycling endosomes to the cell surface to control plasma membrane expansion during cell spreading (Balasubramanian et al., 2010). Therefore, to investigate a role for Myo1c in the trafficking of lipid-raft-associated marker proteins, we compared the cellular distribution of Myo1c and RalA in HeLa cells. In cells expressing HA–RalA alone or HA–RalA and GFP–Myo1c, RalA and endogenous Myo1c or GFP–Myo1c colocalized at the plasma membrane, especially at sites where the membrane was undergoing dynamic rearrangement such as membrane ruffles (Fig. 4A,B, black arrowheads). Furthermore, Myo1c and RalA were enriched along intracellular membrane tubules and vesicles that emanated from the perinuclear region, indicative of the tubular morphology and cellular localization of the endocytic recycling compartment (Fig. 4A,B, white arrowheads). RalA-mediated raft recycling was shown to require its effector ExoC2, a component of the exocyst complex also known as Sec5 (Balasubramanian et al., 2010), and indeed we observe that RalA-positive tubules contained not only Myo1c but also ExoC2 (Fig. 4C). This RalA- and Myo1c-positive tubular compartment was found to be enriched in GPI-anchored proteins, such as CD59, CD55 and the GFP–GPI probe, suggesting that Myo1c associates with endocytic recycling tubules that are highly enriched in lipid-raft-associated marker proteins (Fig. 4D–F; see also Fig. 1C and supplementary material Movie 1) (Eyster et al., 2009; Naslavsky et al., 2004).

Myo1c promotes lipid-raft-enriched membrane tubule formation

In mammalian cells, at least two distinct recycling pathways have been identified whereby tubular carriers bring internalized cargo back to the plasma membrane. In the first pathway, cargo such as the transferrin receptor (TfnR), internalized by clathrin-mediated endocytosis, is recycled back to the cell surface via the well-studied Rab11-positive endocytic recycling compartment. The second pathway, which recycles molecules internalized by clathrin-independent endocytosis, is less well understood, but is typically characterized by the trafficking of GPI-linked raft markers such as CD55 and CD59 (Eyster et al., 2009; Naslavsky et al., 2004).

The localization of Myo1c on membrane tubules emanating from the perinuclear recycling compartment prompted us to investigate whether Myo1c is required for tubule formation in one of these specific recycling pathways. In mock-transfected cells, we frequently observed RalA- and GFP–GPI-positive tubules extending from a perinuclear region to the plasma membrane (Fig. 5A), whereas in Myo1c-knockdown cells these tubules are lost and the RalA- and GPI-containing compartment was redistributed into a condensed perinuclear structure (Fig. 5A); this is similar to the redistribution observed for the lipid-raft-associated caveolin-1, CD59 and CD55 (Fig. 2; supplementary material Fig. S2). Overall the number of cells containing lipid raft tubules was reduced from 37.5±4.9% in mock cells to 19±4.2% (±s.d.) in Myo1c-knockdown cells. Myo1c specifically stabilized only the RalA- and GPI-positive membrane tubules because the morphology and tubular membranes associated with the Rab11-positive recycling compartment was unaffected in Myo1c-knockdown cells (Fig. 5B; supplementary material Fig. S5B–D). Furthermore, loss of Myo1c did not affect the subcellular distribution of TfnR (supplementary material Fig. S5A,B) and no defect in TfnR recycling was observed in cells lacking Myo1c (Fig. 5C,D).

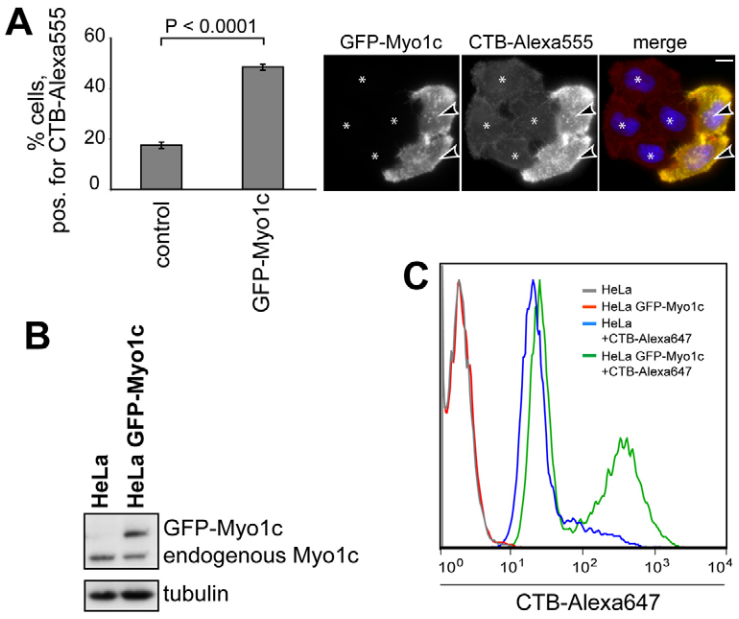

Fig. 3. Overexpression of Myo1c increases surface raft levels. (**A**) Cell surface lipid rafts of HeLa cells transiently transfected with GFP–Myo1c were visualized with CTB–Alexa-Fluor-555. 82% of non-transfected control cells exhibited a modest level of surface CTB staining (indicated by * in the example pictures). Scale bar, 10 μm. Overexpression of GFP–Myo1c increases the percentage of CTB positive cells (arrowheads) from 18% in control cells to 49%. A total number of 2544 cells from three independent experiments were analyzed. Values are means±s.e.m. (**B**) A stable HeLa cell line expressing homogenous levels of GFP–Myo1c was created by FACS sorting. Cell lysates of control HeLa cells and HeLa cells stably expressing GFP–Myo1c were analyzed by SDS-PAGE and immunoblotted with antibodies against Myo1c and α-tubulin, used as a loading control, demonstrating that endogenous and exogenous Myo1c are expressed at similar levels. (**C**) For labeling of cell surface lipid rafts, control HeLa cells and HeLa cells stably expressing GFP–Myo1c were incubated with or without CTB–Alexa-Fluor-647 (CTB-Alexa647), while in suspension. The amount of cell-surface-bound CTB-Alexa647 was determined by FACS analysis.

Previous studies have demonstrated that proteins not associated with lipid rafts such as CD98, CD147 and the class I MHC (MHC-I), can use the same recycling pathway as CD55 and CD59 (Eyster et al., 2009). Interestingly, depletion of Myo1c has a more dramatic effect on the redistribution of lipid-raft-associated cargo than on non-raft proteins CD98 and MHC-I (supplementary material Fig. S2B,C). Similar to Rab11, CD98 and MHC-I showed some colocalization with the collapsed raft-enriched recycling compartment in Myo1c-depleted cells, but the formation of tubular carriers marked by these proteins was not affected (supplementary material Fig. S2B,C, arrowheads).

Collectively these results thus demonstrate that Myo1c is specifically required for the formation of lipid-raft-enriched membrane tubules emanating from a juxtanuclear recycling compartment but is clearly not involved in Rab11-dependent recycling of the TfnR to the plasma membrane.

Myo1c facilitates recycling but not internalization of lipid rafts

Our data so far indicates that Myo1c plays a role in exocytosis and/or recycling of lipid-raft-associated marker proteins to the plasma membrane. To confirm further this observation, automated microscopy was employed to measure the rate of lipid raft recycling in adherent cells using antibodies against CD55. As shown in Fig. 6A, the rate of CD55 antibody recycling is significantly ($P<0.05$) slower in Myo1c-depleted cells as compared with that in mock-treated cells. This lower rate of steady-state raft recycling in Myo1c-depleted cells caused a dramatic accumulation of CD55, as the levels of intracellular CD55 were more than twice as high as those in control cells (Fig. 6B). The total amounts of CD55 expressed in control and Myo1c-knockdown cells, however, are similar as assessed by western blotting (Fig. 6C) and microscopy (data not shown).

The intracellular accumulation of CD55 in Myo1c-depleted cells was due to a defect in exocytosis and/or recycling of lipid raft marker proteins and no changes in the internalization of lipid rafts, labeled with antibodies against CD55 or CD59 were observed by immunofluorescence microscopy (Fig. 6D,E). In both mock-treated and Myo1c-depleted cells antibodies against CD55 and CD59 were internalized at a similar rate, however, in knockdown cells these markers accumulated in the juxtanuclear spot that was previously identified as the collapsed recycling compartment (Figs 4,5; supplementary material Figs S4, S5). The uptake efficiency of lipid-raft-associated CD55 was measured using automated microscopy and imaging software and demonstrated no significant difference in the rate of endocytosis of CD55 (Fig. 6F). These measurements were performed in the presence of primaquine, a drug known to inhibit endocytic recycling.

Myo1c-mediated lipid raft exocytosis is crucial during cell spreading

During cell spreading, the plasma membrane surface area is increased by the exocytosis of membranes enriched in GPI-anchored proteins and other lipid raft markers that are recycled back to the cell surface (Balasubramanian et al., 2010; Balasubramanian et al., 2007; Gauthier et al., 2009). To test whether Myo1c has a role in cell spreading, mock and Myo1c-depleted HeLa cells were seeded onto fibronectin-coated coverslips and allowed to spread for 2 hours. The cells were then fixed, the actin cytoskeleton labeled with Rhodamine–phalloidin and random fields of cells analyzed using Volocity Imaging software to measure the area that the cells had covered during spreading. Representative images of mock-transfected cells or cells transfected with *MYO1C* siRNA are shown in Fig. 7A. Quantification of a total of 5781 cells from three independent experiments showed that cell spreading was reduced by 44.5±7.1% following Myo1c knockdown (Fig. 7B). Similarly, spreading of cells transiently transfected with the non-functional dominant-negative rigor GFP–Myo1c^{K111R} mutant was impaired by 38.1±2.5%. A similar impairment in cell spreading was recently observed in cells expressing non-functional RalA (Balasubramanian et al., 2010).

Cell spreading requires the assembly of focal adhesion contacts that mediate adhesion to the extracellular matrix. In control cells, the focal adhesion markers vinculin and paxillin were enriched in

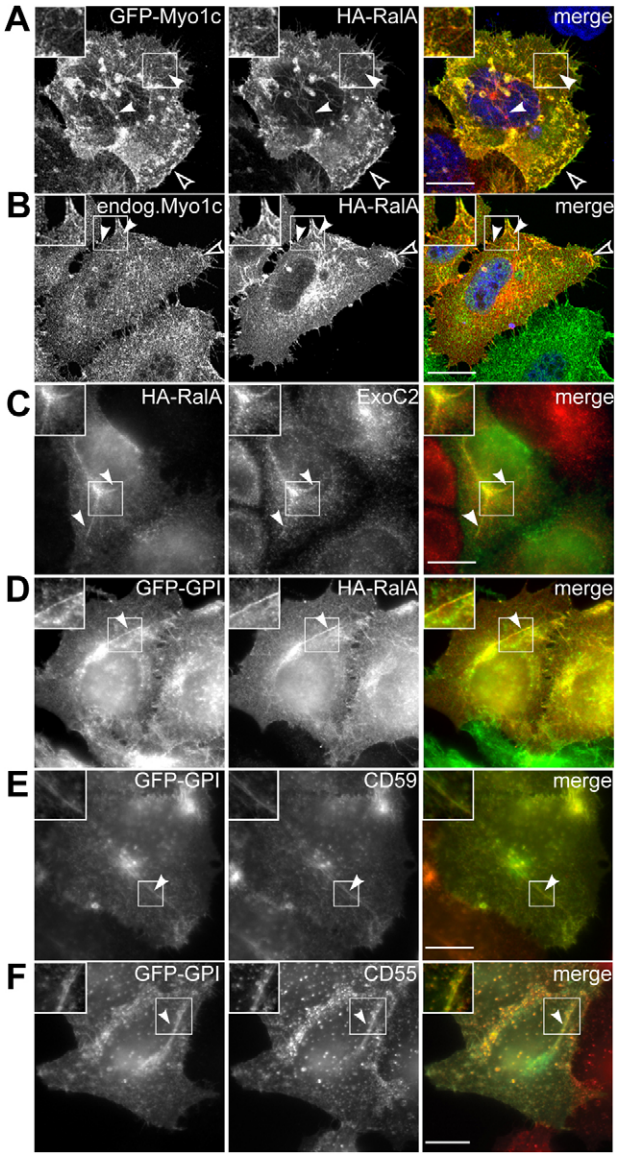

Fig. 4. Myo1c colocalizes with RalA on lipid raft enriched tubules. (**A**) HeLa cells were co-transfected with HA–RalA and GFP–Myo1c, or (**B**) transfected with HA–RalA and stained for HA–RalA and endogenous Myo1c for confocal microscopy. White arrowheads highlight colocalization of Myo1c and RalA on tubules, black arrowheads exemplify colocalization on membrane ruffles of the plasma membrane. Cell nuclei are shown in blue in the merged images. (**C**) HeLa cells expressing HA–RalA were labeled with antibodies against HA and the exocyst component ExoC2. (**D**–**F**) HeLa cells were co-transfected with GFP–GPI and HA–RalA or transfected with GFP–GPI and stained with antibodies against GFP and HA (D), CD59 (E) or CD55 (F). The inserts are enlarged representations of the boxed regions. Scale bars, 10 μm.

numerous discrete foci at the ventral side of the cell (Fig. 7C). By contrast, in Myo1c-knockdown cells, which exhibited a rounded cell morphology, the focal adhesions, labeled with antibodies against vinculin or paxillin, were clustered in a continuous band at the edge of the cell. The same phenotype was observed in cells overexpressing the dominant-negative Myo1c^{K111R} mutant (Fig. 7C) or when Myo1c knockdown was performed through using the four individual smart pool siRNA oligonucleotides individually (supplementary material Fig. S1B). Thus, Myo1c clearly plays a role during cell spreading and impaired cell spreading leads to the accumulation of focal adhesion markers around the edge of the cell.

To determine whether the defect in cell spreading observed in the Myo1c-depleted cells is linked to impaired lipid raft exocytosis, we compared cell surface levels of lipid rafts in control and Myo1c-knockdown cells during cell spreading. After detachment, mock- and Myo1c-depleted cells were held in suspension to encourage lipid raft endocytosis, then reseeded onto fibronectin-coated coverslips and allowed to spread, before fixation and labeling of cell surface lipid rafts with antibodies against CD59 or CD55. Quantification of surface raft levels using Volocity Imaging Software revealed a significant decrease in the amount of the raft markers CD59 (Fig. 7D) and CD55 (Fig. 7E) on the cell surface in Myo1c-depleted cells as compared with that in control cells. These data demonstrate that Myo1c facilitates lipid raft exocytosis during cell spreading.

Myo1c is required for random cell migration

Having established that Myo1c modulates cell spreading owing to its role in lipid raft trafficking, we next investigated whether Myo1c is also required during cell migration. Motile retinal pigment epithelial (RPE) cells were depleted of Myo1c (Fig. 8A) and the random migration of fully spread cells on fibronectin-coated coverslips was captured by time-lapse video microscopy. The motility of more than 240 individual cells in three independent experiments was followed over 3 hours using Volocity tracking software. The single-cell trajectories of one representative experiment are shown in Fig. 8B. Quantitative analysis revealed that the average track length covered by Myo1c-knockdown cells over 3 hours was reduced by over 50% from ~59 μm to ~26 μm compared with that in control cells (Fig. 8C). Similarly, the velocity of movement was reduced; whereas control cells migrated with a speed of ~0.36 μm/minute, in Myo1c knockdown cells the velocity of movement was decreased to ~0.16 μm/minute (i.e. a ~50% reduction) (Fig. 8C). Interestingly, a similar phenotype was observed upon siRNA-mediated depletion of RalA or upon a Myo1c, RalA double knockdown (Fig. 8B,C). We therefore conclude that the loss of Myo1c and its interacting protein RalA negatively impacts upon both the migration speed and the track length of randomly moving cells.

Myo1c promotes ruffle formation required for macropinocytosis and pathogen invasion

The presence of cholesterol-enriched lipid rafts at the plasma membrane recruits activated Rac1, which regulates actin dynamics at the cell surface and stimulates membrane ruffle formation (Balasubramanian et al., 2007; Radhakrishna et al., 1999). These membrane ruffles are not only linked to cell motility but are also required for macropinocytosis, a specialized endocytic mechanism for the uptake of large amounts of fluids. To assess whether the loss of lipid raft domains from the cell surface in Myo1c-knockdown cells has an impact on plasma membrane dynamics and membrane ruffle formation, we measured the rate of macropinocytosis in Myo1c-depleted cells by incubating the cells with fluorescent dextran (70 kDa). Loss of Myo1c reduced the number of cells containing dextran-positive macropinosomes (vesicles larger than 0.5 μm) from 23.2±2.82%

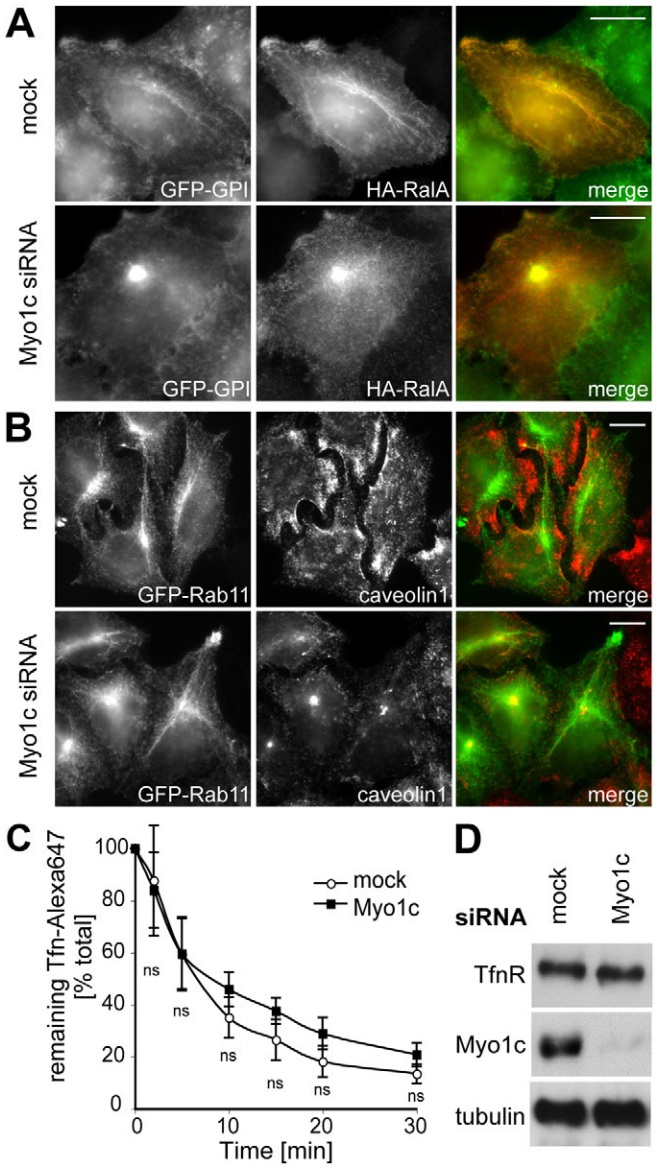

Fig. 5. Myo1c depletion reduces formation of lipid raft enriched tubules, but does not affect recycling of transferrin receptor. (**A**) HeLa cells co-transfected with GFP–GPI and HA–RalA were treated with siRNA targeting *MYO1C* and labeled with antibodies against HA and GFP. (**B**) HeLa cells stably expressing GFP–Rab11 were mock- or Myo1c-depleted and stained with antibodies against GFP and caveolin-1. Scale bars, 10 µm. (**C**) Control and Myo1c-depleted cells were pulsed with Tfn–Alexa-Fluor-647 (Tfn-Alexa647) at 37℃ for 30 minutes, then washed and incubated at 37℃ in the presence of excess unlabeled Tfn for indicated times. The amount of Tfn-Alexa647 remaining in the cell was determined by FACS analysis and expressed as a percentage of total endocytosed Tfn-Alexa647 at time zero. Graphs represent the means±s.d. of three independent experiments. ns, not significant. (**D**) Cell lysates from mock- and Myo1c-depleted HeLa cells were blotted and probed with antibodies against transferrin receptor (TfnR), Myo1c and α-tubulin as a loading control to confirm that mock and knockdown cells express similar levels of TfR.

in control cells to 12.1±1.2% in Myo1c-knockdown cells (Fig. 9A).

Bacterial pathogens like *Salmonella enterica* trigger membrane ruffle formation to invade host cells, a process that requires the delivery of membranes to sites of pathogen entry. To investigate whether Myo1c is recruited to sites of bacterial invasion, HeLa cells stably expressing GFP–Myo1c were infected with *Salmonella enterica* serovar Typhimurium. Infected cells show profound membrane ruffling at sites of *Salmonella* entry and intriguingly, Myo1c was strongly recruited to these invasion ruffles (Fig. 9B), indicating that there is a role for Myo1c in this process. Interestingly, RalA, ExoC2 and the raft marker GFP–GPI also localize to these invasion ruffles (Fig. 9B). To examine further the role of Myo1c during pathogen entry, HeLa cells depleted of Myo1c were infected with *Salmonella enterica* serovar Typhimurium and the efficiency of bacterial invasion was quantified by counting the number of bacterial colonies grown from the infected HeLa cell lysates (Fig. 9C). Interestingly, invasion was inhibited by 34.1±9.1% in Myo1c-knockdown cells. When cells were depleted of RalA, bacteria uptake was reduced by 44.5±6.2%, confirming previous findings by Nichols and Casanova (Nichols and Casanova, 2010). Thus, Myo1c regulates the trafficking of lipid raft microdomains to the cell surface, which has an impact not only on cell spreading and motility but also on other cellular processes that require cholesterol-rich lipid rafts on the plasma membrane, such as macropinocytosis and pathogen invasion.

Discussion

In the cell, the plasticity, composition and surface area of the plasma membrane is controlled by specialized endocytic recycling pathways, which maintain the fine balance between the endocytosis and exocytosis of specific proteins and lipids. Cargo proteins associated with lipid raft membranes are internalized by clathrin-independent endocytosis; however, the molecular determinants that regulate intracellular trafficking in this pathway have yet to be established (Eyster et al., 2009; Grant and Donaldson, 2009). Under steady-state conditions most of the lipid raft markers are at the cell surface, but a small pool of the markers cycles constitutively between the plasma membrane and the Golgi complex (Nichols et al., 2001). When external signals during pathogen entry or cell spreading initiate a rapid remodeling of the plasma membrane, however, internalized lipid raft domains are recycled from a perinuclear storage compartment, which is distinct from the Golgi complex, back to the cell surface (Balasubramanian et al., 2007; Gauthier et al., 2009).

In this study, we have identified Myo1c as a vital component of the machinery that regulates this pathway, as demonstrated after Myo1c knockdown, which induces a dramatic loss of GPI-anchored proteins and raft membranes from the cell surface and their accumulation at a perinuclear location. Indeed, whereas depletion of Myo1c decreases raft levels at the cell surface, its overexpression increases exocytosis of raft markers. Myo1c function in this recycling pathway involves RalA, a known Myo1c-interacting protein (Chen et al., 2007) that regulates the exocytosis of raft domains from a perinuclear recycling compartment to the plasma membrane during cell spreading (Balasubramanian et al., 2010; Gupta et al., 2006). Myo1c and RalA colocalize at the plasma membrane and along dynamic membrane tubules that emanate from the perinuclear recycling compartment and are enriched in GPI-anchored cargo molecules. Our results therefore strongly suggest that Myo1c facilitates raft-enriched cargo delivery to the cell surface through a tubular recycling network.

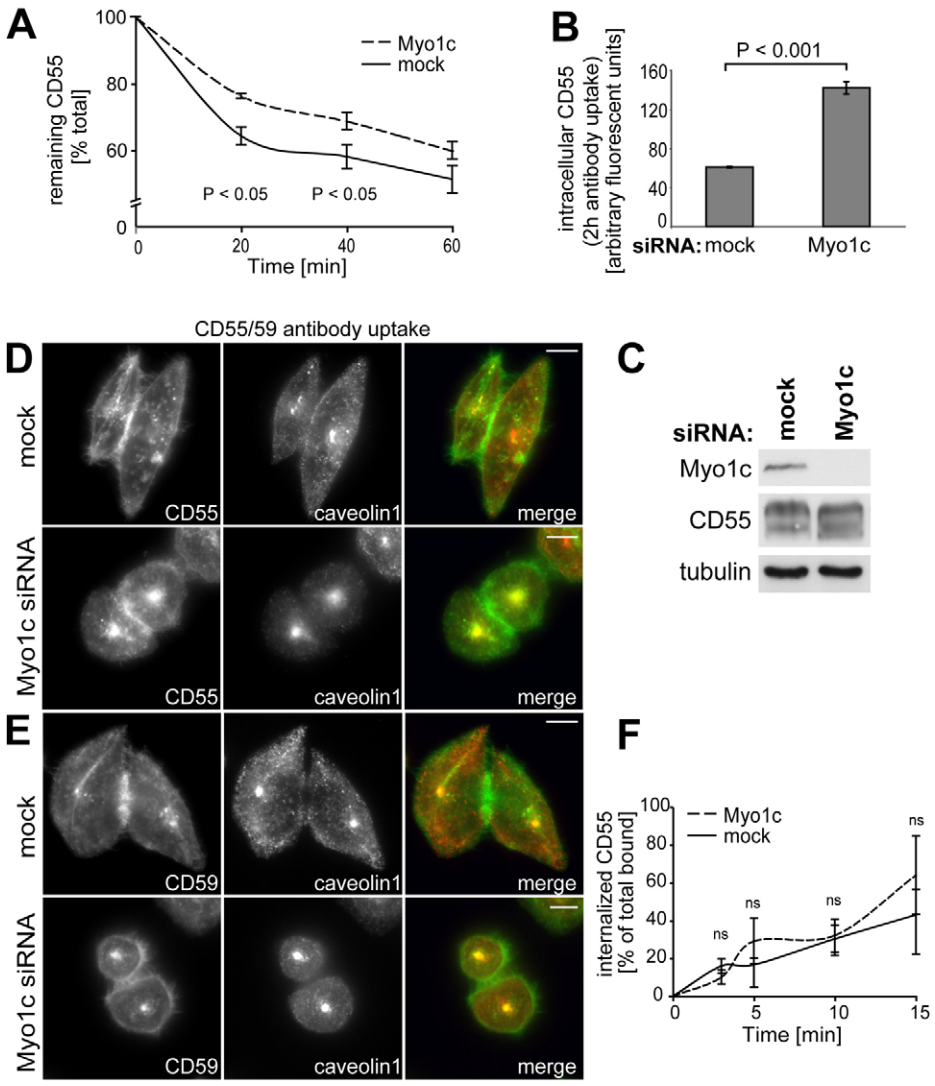

Fig. 6. Myo1c facilitates lipid raft recycling, but is dispensable for lipid raft internalization. (**A**) Control and Myo1c-depleted cells were loaded with antibodies against CD55 at 37℃ for 2 hours. After acid stripping the cells were incubated at 37℃ for indicated times to allow CD55 recycling. The remaining anti-CD55 antibodies were detected with secondary antibodies conjugated to Alexa Fluor 488, quantified by automated microscopy and are expressed as a percentage of total endocytosed CD55 antibodies at time zero. Graphs represent the means±s.e.m. of three independent experiments. A total number of >76,000 cells were quantified, with a minimum of 3000 cells per time point. (**B**) To quantify steady-state levels of intracellular CD55, mock- or Myo1c-depleted cells were incubated for 2 hours with anti-CD55 antibodies. After acid stripping intracellular anti-CD55 antibodies were detected with Alexa-Fluor-488-conjugated secondary antibodies and quantified using automated microscopy. Graphs represent the means±s.e.m. for three independent experiments (>18,000 cells). (**C**) Cell lysates from mock- and Myo1c-depleted HeLa cells were blotted and probed with antibodies against Myo1c, CD55 and α-tubulin, as a loading control, to confirm that mock and knockdown cells express similar levels of CD55. (**D**) Antibodies against CD55 or (**E**) CD59 were taken up into mock- or Myo1c-depleted HeLa cells, before fixation and labeling with antibodies against caveolin-1 for immunofluorescence microscopy. (**F**) Control and Myo1c-knockdown cells were prelabeled with antibodies against CD55 on ice, then incubated at 37℃ for indicated times to allow internalization in the presence of primaquine. Intracellular anti-CD55 antibodies were stained with fluorescently labeled secondary antibodies. Internalized CD55 antibodies are expressed as a percentage of the total amount of anti-CD55 antibodies bound to the cell surface before uptake. Graphs represent the means±s.e.m. of three independent experiments. A total number of >90,000 cells were quantified, with a minimum of 3000 cells per time point. ns, not significant.

Interestingly, an association of Myo1c with lipid raft microdomains was first indicated by proteomics studies, which identified this myosin in purified lipid raft fractions isolated from B-cells (Gupta et al., 2006; Saeki et al., 2003). Similarly, we and Arif et al. (Arif et al., 2011) have shown that Myo1c co-fractionates with lipid raft markers on sucrose gradients after Triton X-100 extraction. Although so far no cargo adaptor proteins have been shown to bind to the Myo1c tail region, phosphoinositides such as Ptd(4,5)InsP_2 bind directly to a putative pleckstrin homology domain in the tail domain (Hokanson et al., 2006; Hokanson and Ostap, 2006). Therefore, Myo1c targeting to lipid rafts is likely to involve Ptd(4,5)InsP_2, which is enriched in these lipid microdomains, and possibly also RalA, which binds to the neck region of this myosin and might serve as a cargo receptor for this myosin. However, lipid association of RalA might be very transient because very little

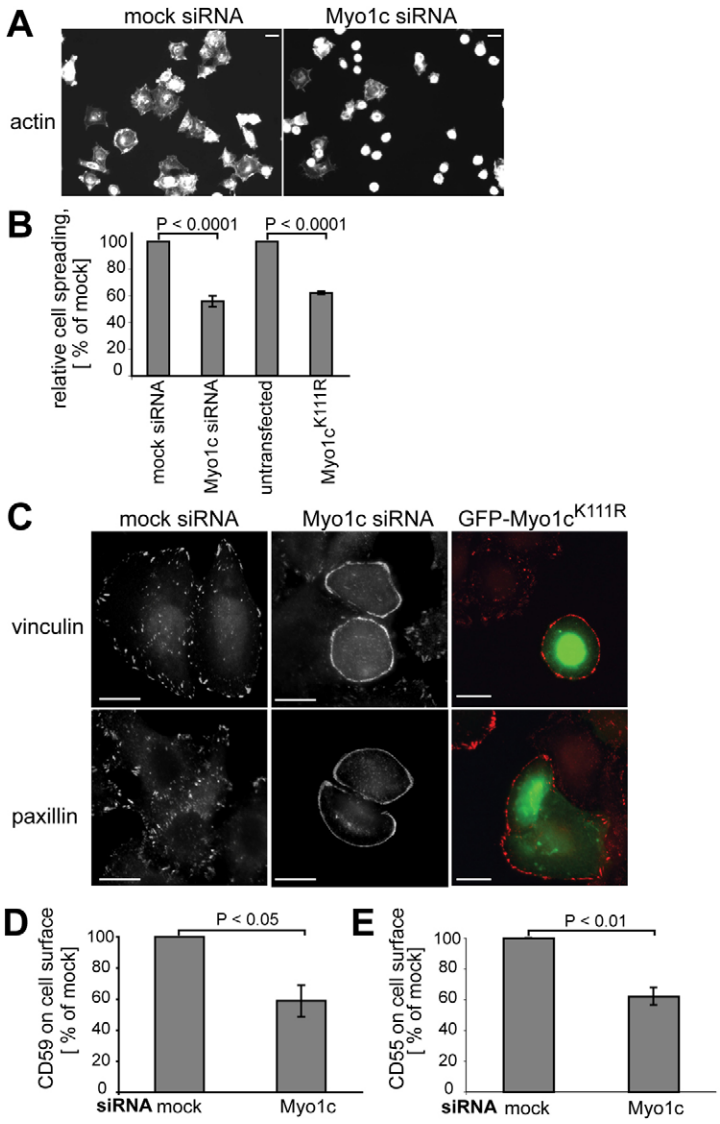

Fig. 7. Myo1c is required for exocytosis of lipid rafts during cell spreading and depletion of Myo1c impairs cell spreading and rearranges focal adhesions. (**A**) HeLa cells, either mock- or Myo1c-depleted, were detached from the tissue culture dish, held in suspension to encourage raft internalization before seeding onto fibronectin-coated coverslips. Their ability to spread after 2 hours was assessed using Rhodamine–phalloidin as a cell label, which stains F-actin. Scale bars, 20 µm. (**B**) For quantification of cell spreading, images of randomly selected fields were taken and the mean area covered by cells was measured using Volocity Imaging software. A total of 5781 cells from three independent experiments were analyzed. Values are means±s.e.m. (**C**) HeLa cells, either mock- or Myo1c-depleted, or transiently transfected with the GFP–Myo1c^{K111R} rigor mutant, were labeled with antibodies against the focal adhesion markers vinculin or paxillin. Scale bars, 20 µm. (**D**,**E**) Mock- and Myo1c-depleted HeLa cells were detached, held in suspension, reseeded onto fibronectin-coated coverslips and allowed to spread for 3 hours. Cell surface lipid rafts were labeled with antibodies against CD59 (D) or CD55 (E) and secondary antibodies conjugated to Alexa Fluor 555. For quantification of surface rafts, randomly selected fields were captured and the total fluorescence intensity per cell was measured using Volocity Imaging software. A total number of 1213 cells from three independent experiments (D) and 848 cells from three independent experiments (E) were analyzed. Values are means±s.e.m.

RalA partitioned into raft fractions in our flotation assay, indicating that RalA is not involved in the lipid raft recruitment of Myo1c.

The key role of Myo1c in the trafficking of lipid raft associated proteins, as well as the localized delivery of cholesterol and sphingolipid-enriched membranes, is the regulation of cell spreading, cell migration, macropinocytosis and *Salmonella* invasion. All these processes depend on active plasma membrane remodeling and expansion and suggest that there is a synergy between Myo1c and RalA. For example, RalA has recently been shown to be necessary for exocyst-dependent membrane delivery for *Salmonella* uptake by membrane ruffles (Nichols and Casanova, 2010). We confirmed this observation and further showed that RalA accumulates at *Salmonella* invasion sites and promotes pathogen-induced macropinocytosis. These invasion ruffles are also enriched in both Myo1c and raft membranes, indicating that Myo1c is required for bacterial invasion. In this process, Myo1c might regulate the recycling of membranes to enable plasma membrane expansion for pathogen uptake and it might also deliver membrane-raft-associated signaling molecules to the plasma membrane. Defective raft trafficking has been shown to lead to the mislocalization of the Rho GTPases Rac1 and Cdc42 and block *Salmonella*-induced macropinocytosis (Misselwitz et al., 2011).

So how does Myo1c mediate raft trafficking and where along the recycling pathway is Myo1c required? In the specialized lipid raft recycling pathway studied here, activation of Arf6 is believed to drive exit from the recycling endosome, whereas RalA and the exocyst complex mediate docking at the plasma membrane (Balasubramanian et al., 2010; Balasubramanian et al., 2007; Radhakrishna et al., 1999; Radhakrishna and Donaldson, 1997). The majority of Myo1c is present at the plasma membrane, concentrated in actin-rich regions such as filopodia and membrane ruffles (Bose et al., 2004; Diefenbach et al., 2002; Ruppert et al., 1995; Wagner et al., 1992; Wagner et al., 2005). However, in a number of cell types, endogenous Myo1c is also distributed throughout the cytoplasm in a punctate pattern (Ruppert et al., 1995; Wagner et al., 1992). We observed that Myo1c, RalA and the exocyst are present at the plasma membrane and also on tubular carriers emanating from the

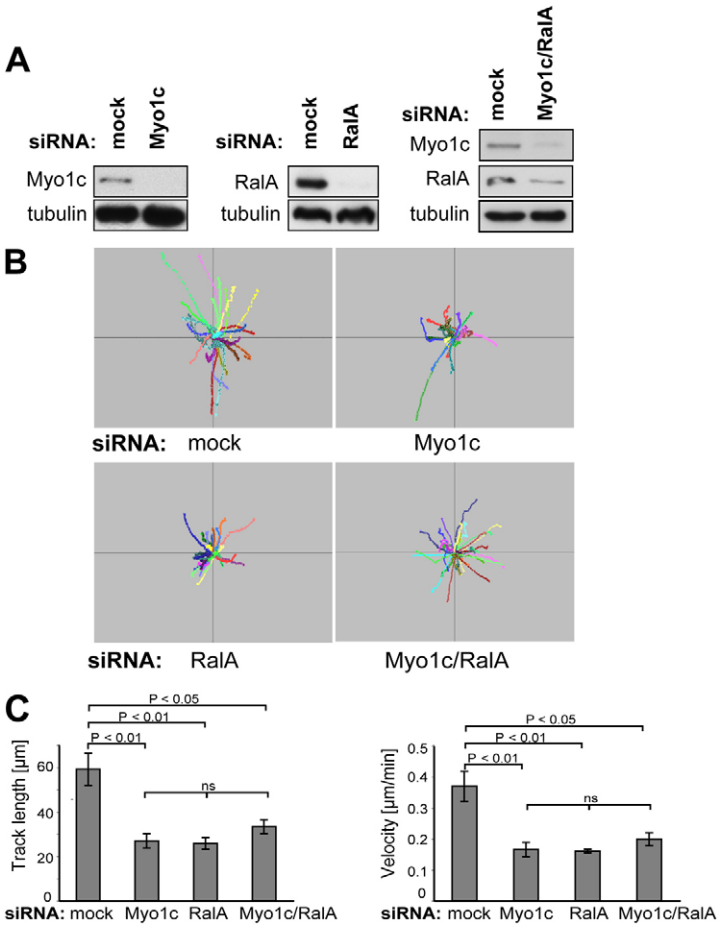

Fig. 8. Random migration requires Myo1c and RalA. (**A**) Mock, Myo1c, RalA and both Myo1c and RalA were depleted through siRNA treatment in RPE cells, which were then lysed, blotted and probed with antibodies against Myo1c, RalA and α-tubulin, as a loading control, to confirm the successful protein knockdown. Single knockdowns of either Myo1c or RalA led to a near complete protein depletion with undetectable levels of Myo1c or RalA by western blotting. However, in the double-knockdown protein depletion was less efficient as shown in the representative immunoblots. (**B**) Time-lapse video microscopy was used to capture the movements of individual control, Myo1c and RalA single-knockdown and Myo1c and RalA double-knockdown cells on fibronectin-coated coverslips over 3 hours. Migration tracks of 249 cells from at least three independent experiments per knockdown were analyzed using Volocity Imaging software. Individual cell trajectories of one representative experiment are depicted. (**C**) Quantification revealed that loss of Myo1c, RalA or Myo1c in combination with RalA significantly reduces migration speed and track length. Values are means±s.e.m. ns, not significant.

perinuclear recycling pathway, and that loss of Myo1c causes the collapse of these recycling carriers into the perinuclear membrane compartment.

The localization of Myo1c is mirrored by the distribution of its lipid anchor Ptd(4,5)InsP_2, which is found at the plasma membrane and also in recycling tubules (Brown et al., 2001). Thus, the dual localization of Myo1c on recycling tubules and at the plasma membrane suggests possible multiple functions for this myosin during lipid raft exocytosis. First, it could be involved in tubule formation or cargo sorting at the recycling endosome. Cargo is recycled back to the plasma membrane using at least two distinct recycling pathways, one to transport GPI-anchored proteins and lipid-raft-associated cargo and a second separate pathway for recycling of cargo internalized by clathrin-dependent endocytosis such as the TfnR and the low-density lipoprotein (LDL) receptor (Grant and Donaldson, 2009). Sorting is an important process at the perinuclear recycling compartment and Myo1c could be part of the sorting machinery that clusters or concentrates lipid-raft-associated cargo by anchoring specific membrane domains to the surrounding actin cytoskeleton. This hypothesis is supported by our observation that loss of Myo1c changes the distribution of GPI-anchored proteins including CD55 and CD59, but has less effect on trafficking of non-raft cargoes such as CD98 and MHC-I. In addition, Myo1c could promote tubule formation in the perinuclear region by anchoring and pulling the specific membranes along actin filaments to form tubules, which are then transported towards the plasma membrane by kinesin motors moving along the microtubule network. Similar to its function in transport of GLUT4-positive vesicles in adipocytes (Bose et al., 2002; Bose et al., 2004), Myo1c could also mediate the final steps during exocytosis through the cortical actin network beneath the plasma membrane, where Myo1c might promote the delivery and fusion of lipid-raft-containing membranes with the plasma membrane.

What type of motor protein is Myo1c and how is it adapted to carry out these specific cellular functions? In vitro kinetic and single-molecule optical trap studies have shown that Myo1c is a slow monomeric myosin that remains attached to actin during most of its duty (ATPase) cycle, indicating that it is likely to have an anchoring, membrane stabilizing and tension generating role rather than a role in rapidly transporting cargo (Batters et al., 2004a; Batters et al., 2004b). Unlike the other myosins that have been studied in some detail, such as myosin V, VI and VII, which have a wide range of tail-binding cargo and/or adaptor proteins, no such adaptor proteins have been shown to bind to the Myo1c tail. Instead the Myo1c tail binds specifically to Ptd(4,5)InsP_2 through a pleckstrin homology domain site with a β1-loop-β2 motif (Hokanson et al., 2006; Hokanson and Ostap, 2006). Mutation of two basic residues within this motif abolishes binding of Myo1c to Ptd(4,5)InsP_2 in vitro and binding to the plasma membrane in vivo (Hokanson et al., 2006; Hokanson and Ostap, 2006). A number of proteins however including RalA, calcium-binding protein 1 and phosphoprotein regulator 14-3-3 have been shown to bind to the IQ motifs in the regulatory neck

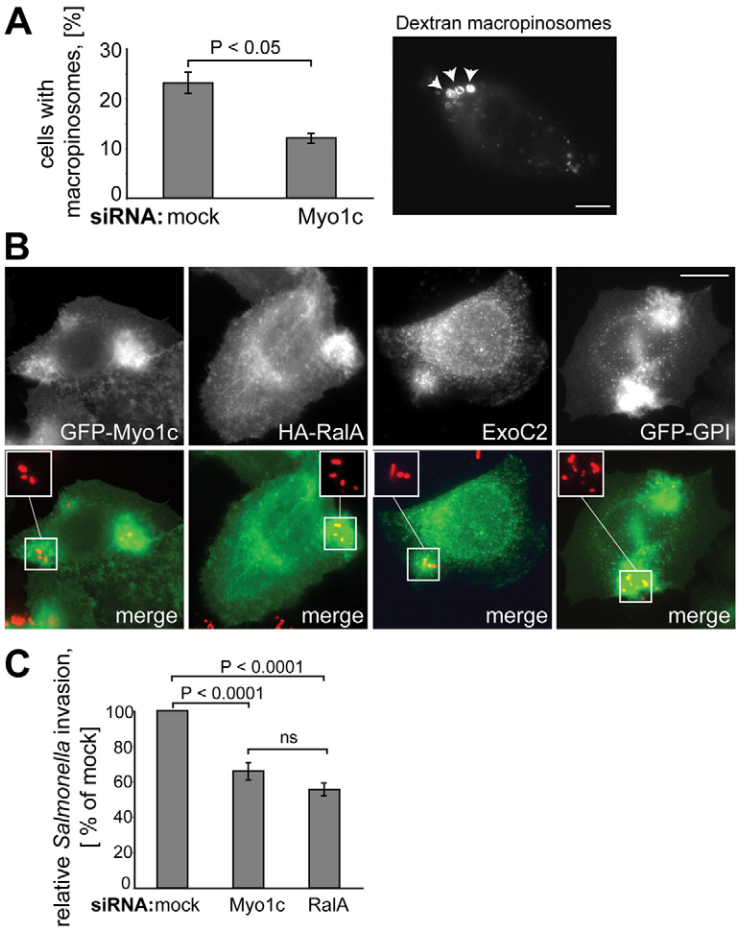

Fig. 9. Myo1c depletion impairs membrane ruffle formation crucial for macropinocytosis and *Salmonella* invasion. (**A**) To quantify membrane ruffling, mock- and *MYO1C*-siRNA-treated A549 cells were loaded with 70 kDa TMR-coupled dextran and the number of cells containing dextran-positive structures larger than 0.5 µm in size were quantified. A representative picture of one cell containing three dextran macropinosomes (arrowheads) is shown. A total number of 2611 cells from three independent experiments were analyzed. Values presented are means±s.e.m. (**B**) HeLa cells transiently transfected with GFP–Myo1c, HA–RalA or GFP–GPI were infected with wild-type *Salmonella* Typhimurium labeled with Alexa555 conjugated succinimidyl-esters and stained with antibodies against GFP, HA and endogenous ExoC2. The merged images (bottom panel) show bacteria in red. The inserts are enlarged, single colour representations of the white boxes. Bars, 10 µm (**C**) Mock, Myo1c and RalA siRNA treated HeLa cells were infected with *Salmonella enterica* serovar Typhimurium for 1 hour. After a gentamicin protection assay to kill extracellular bacteria, invasion was quantified by spreading cell lysates onto LB agar for counting of bacterial colony forming units. Invasion efficiency is presented as a percentage normalized to mock depleted cells. Values are means±s.e.m. for four independent experiments, each performed in triplicate. ns, non-significant.

region of Myo1c (Chen et al., 2007; Tang et al., 2002; Tang et al., 2007; Yip et al., 2008). In the cell, Myo1c might spend most of its time associated to lipid membranes through its tail domain while it is bound to actin filaments by its motor domain. In the exocytic pathway studied here, activated RalA binding to the regulatory neck region between the motor and tail domains might act as regulatory 'switch' to modulate these interactions. Therefore, the cellular functions of Myo1c might be controlled by the binding of its tail to Ptd(4,5)InsP_2 clusters, known to localize at specific sites in membranes and in the presence of Ca^{2+} by the binding of RalA to the regulatory neck region. Thus, Myo1c might facilitate raft trafficking by pulling, anchoring and stabilizing Ptd(4,5)InsP_2-rich membranes on actin filaments, which enable dynamic events, such as membrane tubulation and fusion with the plasma membrane, to occur.

Materials and Methods

Plasmid constructs and antibodies

Full-length human *MYO1C* cDNA (image clone 6144867) was obtained from Source BioScience, Cambridge, UK, amplified by PCR using oligonucleotides containing restriction enzyme sites (XhoI and BamHI or SacII, respectively) and ligated into pEGFPC1 and p_mCherryC1 (Clontech, Mountain View, CA, USA). The rigor mutant K111R was generated using the QuikChange site-directed mutagenesis kit (Stratagene). GFP–GPI was engineered by fusing the signal sequence of CD55 (a gift from Andrew Peden, University of Cambridge, Cambridge, UK) to the N-terminus of GFP and the GPI anchor of CD55 to the C-terminus of GFP. RalA was a gift from Channing Der, University of North Carolina, Chapel Hill, NC (Lim et al., 2006), and was amplified by PCR to add *Xho*I and *Bam*HI restriction enzyme sites and the HA-tag sequence and ligated into pCDNA3.1 (Invitrogen, Paisley, UK). GFP–Rab11 was kindly provided by Matthew Seaman, University of Cambridge, Cambridge, UK. To generate constructs for stable expression, inserts were subcloned into pIRESneo2 (Clontech, USA). All constructs were validated by sequencing using Source BioScience.

The following commercial antibodies were used: rabbit polyclonal antibodies against GFP (Molecular Probes), Myo1c and actin (Sigma-Aldrich), ezrin (Abcam), caveolin-1 and calnexin (Santa Cruz Biotechnology), PLAP (Rockland, USA), ExoC2 (Proteintech, Chicago, IL); mouse monoclonal antibodies against GFP (Abcam), HA (Covance, Princeton, NJ), CD55 (Santa Cruz Biotechnology), CD59 (Calbiochem), MHC-I (W6/32; kind gift from Paul Lehner, University of Cambridge), vinculin and tubulin (Sigma-Aldrich), caveolin-1, flotillin-1 and -2, GM130, CD98 and RalA (BD Biosciences), TfnR (Zymed); sheep polyclonal antibodies against TGN46 (Serotech, Toronto, Canada).

Cell culture, transfection and siRNA

HeLaM cells (Tiwari et al., 1987) were grown in RPMI 1640, RPE cells in 50:50 DMEM:F12 Ham medium and A549 cells in DMEM, all containing 10% FCS, 2 mM L-glutamine, 100 U/ml penicillin and 100 µg/ml streptomycin in a 5% humidified atmosphere. Cells were transfected using FuGENE (Roche Diagnostics) according to the manufacturer's instructions. To generate stably expressing cell lines, HeLa cells were transfected with constructs in pIRESneo2 and selected in medium containing 500 µg/ml G418 (Gibco, Paisley, UK). Expressing cells were enriched by FACS. All siRNA oligonucleotides (ON-TARGETplus) were obtained from Dharmacon (Cramlington, UK). For efficient protein depletion cells were transfected twice with siRNA on day 1 and 3 using OligofectAMINE (Invitrogen). On day 5 cells were processed for corresponding assays. The efficiency of protein knockdown was assessed by immunoblotting.

Immunoblotting

Cells were lysed in SDS loading buffer (2% SDS, 30% glycerol, 1 M β-mercaptoethanol, 6 M urea, 0.125 M Tris pH 6.8, 0.01% Bromophenol Blue), and analyzed by SDS-PAGE followed by immunoblotting with the indicated antibodies. Blots were developed using the ECL detection reagent (GE Healthcare).

Flotation assay

To label surface lipid rafts, cells were cooled and incubated with 4 μg/ml CTB–HRP conjugate (Sigma-Aldrich) on ice for 1 hour. Cells were washed and lysed in cold TNE buffer (20 mM Tris-HCl pH 8.5, 150 mM NaCl, 5 mM EDTA) containing 1% Triton X-100 (Pierce, Cramlington, UK) and Complete™ protease inhibitor cocktail (Roche Diagnostics). Samples were homogenized using a Dounce homogenizer and brought to 40% sucrose and over-layered with a decreasing step sucrose gradient (35–5%), followed by centrifugation at 42,000 rpm, 4℃, 18 hours in a SW 40Ti swinging bucket rotor (Beckman). 10 fractions were harvested from the top of the gradient and aliquots run on an SDS-PAGE and either Coomassie stained or analyzed by immunoblotting. For dot-blot analysis two microliters of each fraction were directly spotted onto a nitrocellulose membrane, before development using the ECL detection reagent.

Immunofluorescence

Cells grown on coverslips were fixed with 4% PFA (or ice-cold methanol for flotillin labeling), permeabilized with 0.2% Triton X-100 and quenched with 10 mM glycine. Fixed cells were blocked with 1% BSA in PBS and processed for indirect immunofluorescence using primary antibodies (as specified in the figure legends) followed by secondary antibodies coupled to Alexa Fluor 488 or Alexa Fluor 568 (Molecular Probes). F-actin was visualized using Rhodamine-coupled phalloidin (Sigma-Aldrich). Surface lipid rafts were labeled using CTB–Alexa-Fluor-555 conjugate and cell nuclei were stained with DAPI (both Invitrogen). TfnR was visualized using human Tfn conjugated to Alexa Fluor 555 (Molecular Probes). Images were obtained at a magnification of 63× using a Zeiss LSM510 META confocal microscope, a Zeiss LSM710 confocal microscope or a Zeiss Axioplan epifluorescence microscope (Zeiss, Jena, Germany), equipped with a Hamamatsu Orca R2 camera (Hamamatsu Photonics, Shizuoka, Japan). Data obtained were analyzed using Volocity 5.2 software (PerkinElmer). For the macropinocytosis assay, cells plated at low density on coverslips were serum starved for 6 hours before incubating for 30 minutes with 0.5 mg/ml of 70 kDa TMR-coupled lysine-fixable dextran (Molecular Probes) in the presence of 20 ng/ml EGF. To quantify cell spreading, cells were detached using enzyme free cell dissociation buffer (Gibco), seeded onto fibronectin-coated (20 μg/ml) coverslips, allowed to spread for 2 hours before fixation and actin labeling. For semi-automated quantification, randomly selected fields were captured on an Improvision Open Lab deconvolusion microscope. The mean area covered by cells was measured using the Volocity 5.2 Imaging Software (PerkinElmer). To quantify cell surface lipid raft levels, cells were processed as for the spreading assay, but allowed to spread for 3 hours. After fixation surface rafts were labeled with antibodies against CD55 or CD59 and Alexa-Fluor-555-coupled secondary antibodies. Randomly selected fields were captured and Volocity Imaging Software was used to calculate the total CD55 or CD59 surface fluorescence per cell.

Spinning disc live-cell microscopy

Cells were grown on coverslips and imaged at 37℃ in CO_2-independent medium (Invitrogen). Images were obtained on a Zeiss Cell Observer SD microscope (Zeiss, Jena, Germany) using a 100× lens and acquired with a Hamamatsu EM-CCD Digital Camera (Hamamatsu Photonics, Shizuoka, Japan) and AxioVision imaging software, version 4.8 (Zeiss).

Lipid raft internalization and recycling assay

For the internalization assay antibodies against CD55 were bound on ice to cell surface receptors. Cells were then incubated at 37℃ for indicated times to allow internalization in the presence of 300 μM primaquine (Sigma-Aldrich) to inhibit recycling. Cell-surface-bound antibodies were removed by acid stripping for 4 minutes in 0.5 M NaCl and 0.2 M acetic acid, before fixation and permeabilization for immunofluorescence as described above. Internalized anti-CD55 antibodies were detected with secondary antibodies conjugated to Alexa Fluor 488 and cell nuclei were stained using DAPI.

For the raft recycling assay, cells were incubated for 2 hours at 37℃ in with antibodies against CD55. Antibodies were removed from the cell surface by acid wash, before incubation at 37℃ for indicated times to allow CD55 recycling. After a second acid strip to remove recycled antibodies from the cell surface, cells were processed for immunofluorescence as described above to detect intracellular CD55.

For the internalization and recycling assays the levels of CD55 were quantified using a fully automated ArrayScan VTi High Content Screening Microscope (Cellomics, Pennsylvania, USA) and imaging software (TargetActivation4 algorithm). The fluorescent signal was normalized to cell numbers using the DAPI stain. A minimum of 3000 cells was analyzed per single timepoint and per condition. Graphs represent three individual knockdown experiments.

FACS-based transferrin recycling assay

Transferrin recycling assays were performed as described previously (Peden et al., 2004). Cells were incubated with Tfn–Alexa-Fluor-647 for 30 minutes at 37℃, washed and incubated at 37℃ with 100 μg/ml unlabeled transferrin (Sigma-Aldrich) for various time points before fixation. Levels of cell-associated Tfn–Alexa-Fluor-647 were determined by FACS analysis using a BD FACS Calibur flow cytometer using CellQuest software (BD Pharmingen). Flow cytometry data was analyzed with FlowJo 8.4 Software.

FACS-based cell surface raft quantification

Cells were detached using enzyme-free cell dissociation buffer (Gibco) and held in suspension before cooling them. Surface rafts of suspended cells were labeled with CTB–Alexa-Fluor-647 (Molecular Probes) on ice for 60 minutes. Then cells were washed and fixed for FACS analysis.

Migration assay

To assess random migration, cells were labeled with 10 μM of Cell Tracker CMRA (Invitrogen) for 30 minutes according to the manufacturer's instructions. Labeled cells were detached using enzyme-free cell dissociation buffer (Gibco), plated onto fibronectin-coated coverslips and left for 2 hours to adhere completely before time-lapse video analysis. Cells were visualized on an Improvison OpenLab deconvolusion microscope (magnification 20×) in a heated environmental chamber (37℃, 5% CO_2) using a Hamamatsu Orca ER camera (Hamamatsu Photonics, Shizuoka, Japan). Images of cells were taken at 2-minute intervals over 3 hours. Migration tracks were analyzed using the Volocity 5.2 Imaging Software (PerkinElmer).

Salmonella invasion

Wild-type *Salmonella enterica* serovar Typhimurium SL1344 were grown in LB broth for 16 hours at 37℃. Bacteria were then subcultured and grown till they reached an OD600 of 2. For immunofluorescence, bacteria were labeled with Alexa-Fluor-555-conjugated succinimidyl esters (Invitrogen) according to the manufacturer's instructions. The inoculum was diluted in RPMI medium supplemented with 2 mM L-glutamine and added to serum-starved cells at a multiplicity of infection (MOI) of 5. For the invasion assay cells were washed after 1 hour of infection and the medium replaced with RPMI containing 20 μg/ml gentamicin to kill extracellular bacteria for 1 hour. Cells were then lysed in PBS containing 0.5% Triton X-100 and 10 mM Tris-HCl pH 7.4. Bacterial dilutions were made in PBS and plated onto LB- agar plates for quantification of bacterial colony forming units. Experiments were performed in triplicates.

Statistical significance

Comparisons between two data points were made using Student's *t*-test, between three or more data points using ANOVA combined with post-hoc Bonferroni's multiple comparison test (GraphPad Prism 5.01).

Acknowledgements

We thank M. N. Seaman and D. A. Tumbarello for critical reading of the manuscript and M. Gratian and M. Bowen for assistance with microscopy and image analysis. We acknowledge J. P. Luzio for helpful discussion, M. V. Chibalina, S. D. Arden, C. Puri and P. Kozik for technical advice and R.A. Floto for support with the *Salmonella* experiments.

Funding

This work was funded by the Wellcome Trust [grant numbers 082870/Z/07/Z to H.B. and 086743 to F.B.]; and the Medical Research Council. The Cambridge Institute for Medical Research is in receipt of a strategic award [grant number 079895/Z/06/Z] from the Wellcome Trust. Deposited in PMC for release after 6 months.

Supplementary material available online at
http://jcs.biologists.org/lookup/suppl/doi:10.1242/jcs.097212/-/DC1

References

Arif, E., Wagner, M. C., Johnstone, D. B., Wong, H. N., George, B., Pruthi, P. A., Lazzara, M. J. and Nihalani, D. (2011). Motor protein myo1c is a podocyte protein that facilitates the transport of slit diaphragm protein neph1 to the podocyte membrane. *Mol. Cell. Biol.* **31**, 2134-2150.

Aschenbrenner, L., Naccache, S. N. and Hasson, T. (2004). Uncoated endocytic vesicles require the unconventional myosin, Myo6, for rapid transport through actin barriers. *Mol. Biol. Cell* **15**, 2253-2263.

Balasubramanian, N., Scott, D. W., Castle, J. D., Casanova, J. E. and Schwartz, M. A. (2007). Arf6 and microtubules in adhesion-dependent trafficking of lipid rafts. *Nat. Cell Biol.* **9**, 1381-1391.

Balasubramanian, N., Meier, J. A., Scott, D. W., Norambuena, A., White, M. A. and Schwartz, M. A. (2010). RalA-exocyst complex regulates integrin-dependent membrane raft exocytosis and growth signaling. *Curr. Biol.* **20**, 75-79.

Batters, C., Arthur, C. P., Lin, A., Porter, J., Geeves, M. A., Milligan, R. A., Molloy, J. E. and Coluccio, L. M. (2004a). Myo1c is designed for the adaptation response in the inner ear. *EMBO J.* **23**, 1433-1440.

Batters, C., Wallace, M. I., Coluccio, L. M. and Molloy, J. E. (2004b). A model of stereocilia adaptation based on single molecule mechanical studies of myosin I. *Philos. Trans. R. Soc. Lond. B Biol. Sci.* **359**, 1895-1905.

Bose, A., Guilherme, A., Robida, S. I., Nicoloro, S. M., Zhou, Q. L., Jiang, Z. Y., Pomerleau, D. P. and Czech, M. P. (2002). Glucose transporter recycling in response to insulin is facilitated by myosin Myo1c. *Nature* **420**, 821-824.

Bose, A., Robida, S., Furcinitti, P. S., Chawla, A., Fogarty, K., Corvera, S. and Czech, M. P. (2004). Unconventional myosin Myo1c promotes membrane fusion in a regulated exocytic pathway. *Mol. Cell Biol.* **24**, 5447-5458.

Brown, D. A. and Rose, J. K. (1992). Sorting of GPI-anchored proteins to glycolipid-enriched membrane subdomains during transport to the apical cell surface. *Cell* **68**, 533-544.

Brown, F. D., Rozelle, A. L., Yin, H. L., Balla, T. and Donaldson, J. G. (2001). Phosphatidylinositol 4,5-bisphosphate and Arf6-regulated membrane traffic. *J. Cell Biol.* **154**, 1007-1017.

Chen, X. W., Leto, D., Chiang, S. H., Wang, Q. and Saltiel, A. R. (2007). Activation of RalA is required for insulin-stimulated Glut4 trafficking to the plasma membrane via the exocyst and the motor protein Myo1c. *Dev. Cell* **13**, 391-404.

del Pozo, M. A., Alderson, N. B., Kiosses, W. B., Chiang, H. H., Anderson, R. G. and Schwartz, M. A. (2004). Integrins regulate Rac targeting by internalization of membrane domains. *Science* **303**, 839-842.

del Pozo, M. A., Balasubramanian, N., Alderson, N. B., Kiosses, W. B., Grande-Garcia, A., Anderson, R. G. and Schwartz, M. A. (2005). Phospho-caveolin-1 mediates integrin-regulated membrane domain internalization. *Nat. Cell Biol.* **7**, 901-908.

Diefenbach, T. J., Latham, V. M., Yimlamai, D., Liu, C. A., Herman, I. M. and Jay, D. G. (2002). Myosin 1c and myosin IIB serve opposing roles in lamellipodial dynamics of the neuronal growth cone. *J. Cell Biol.* **158**, 1207-1217.

Eidels, L., Proia, R. L. and Hart, D. A. (1983). Membrane receptors for bacterial toxins. *Microbiol. Rev.* **47**, 596-620.

Eyster, C. A., Higginson, J. D., Huebner, R., Porat-Shliom, N., Weigert, R., Wu, W. W., Shen, R. F. and Donaldson, J. G. (2009). Discovery of new cargo proteins that enter cells through clathrin-independent endocytosis. *Traffic* **10**, 590-599.

Foster, L. J., De Hoog, C. L. and Mann, M. (2003). Unbiased quantitative proteomics of lipid rafts reveals high specificity for signaling factors. *Proc. Natl. Acad. Sci. USA* **100**, 5813-5818.

Foth, B. J., Goedecke, M. C. and Soldati, D. (2006). New insights into myosin evolution and classification. *Proc. Natl. Acad. Sci. USA* **103**, 3681-3686.

Gauthier, N. C., Rossier, O. M., Mathur, A., Hone, J. C. and Sheetz, M. P. (2009). Plasma membrane area increases with spread area by exocytosis of a GPI-anchored protein compartment. *Mol. Biol. Cell* **20**, 3261-3272.

Gillespie, P. G. and Cyr, J. L. (2004). Myosin-1c, the hair cell's adaptation motor. *Annu. Rev. Physiol.* **66**, 521-545.

Grant, B. D. and Donaldson, J. G. (2009). Pathways and mechanisms of endocytic recycling. *Nat. Rev. Mol. Cell Biol.* **10**, 597-608.

Gupta, N., Wollscheid, B., Watts, J. D., Scheer, B., Aebersold, R. and DeFranco, A. L. (2006). Quantitative proteomic analysis of B cell lipid rafts reveals that ezrin regulates antigen receptor-mediated lipid raft dynamics. *Nat. Immunol.* **7**, 625-633.

Hokanson, D. E. and Ostap, E. M. (2006). Myo1c binds tightly and specifically to phosphatidylinositol 4,5-bisphosphate and inositol 1,4,5-trisphosphate. *Proc. Natl. Acad. Sci. USA* **103**, 3118-3123.

Hokanson, D. E., Laakso, J. M., Lin, T., Sept, D. and Ostap, E. M. (2006). Myo1c binds phosphoinositides through a putative pleckstrin homology domain. *Mol. Biol. Cell* **17**, 4856-4865.

Hope, H. R. and Pike, L. J. (1996). Phosphoinositides and phosphoinositide-utilizing enzymes in detergent-insoluble lipid domains. *Mol. Biol. Cell* **7**, 843-851.

Krendel, M. and Mooseker, M. S. (2005). Myosins: tails (and heads) of functional diversity. *Physiology (Bethesda)* **20**, 239-251.

Legler, D. F., Doucey, M. A., Schneider, P., Chapatte, L., Bender, F. C. and Bron, C. (2005). Differential insertion of GPI-anchored GFPs into lipid rafts of live cells. *FASEB J.* **19**, 73-75.

Lim, K. H., O'Hayer, K., Adam, S. J., Kendall, S. D., Campbell, P. M., Der, C. J. and Counter, C. M. (2006). Divergent roles for RalA and RalB in malignant growth of human pancreatic carcinoma cells. *Curr. Biol.* **16**, 2385-2394.

McKenna, J. M. and Ostap, E. M. (2009). Kinetics of the interaction of myo1c with phosphoinositides. *J. Biol. Chem.* **284**, 28650-28659.

Misselwitz, B., Dilling, S., Vonaesch, P., Sacher, R., Snijder, B., Schlumberger, M., Rout, S., Stark, M., von Mering, C., Pelkmans, L. and Hardt, W. D. (2011). RNAi screen of Salmonella invasion shows role of COPI in membrane targeting of cholesterol and Cdc42. *Mol. Syst. Biol.* **7**, 474.

Naslavsky, N., Weigert, R. and Donaldson, J. G. (2004). Characterization of a nonclathrin endocytic pathway: membrane cargo and lipid requirements. *Mol. Biol. Cell* **15**, 3542-3552.

Nichols, B. J., Kenworthy, A. K., Polishchuk, R. S., Lodge, R., Roberts, T. H., Hirschberg, K., Phair, R. D. and Lippincott-Schwartz, J. (2001). Rapid cycling of lipid raft markers between the cell surface and Golgi complex. *J. Cell Biol.* **153**, 529-541.

Nichols, C. D. and Casanova, J. E. (2010). Salmonella-directed recruitment of new membrane to invasion foci via the host exocyst complex. *Curr. Biol.* **20**, 1316-1320.

Peden, A. A., Schonteich, E., Chun, J., Junutula, J. R., Scheller, R. H. and Prekeris, R. (2004). The RCP-Rab11 complex regulates endocytic protein sorting. *Mol. Biol. Cell* **15**, 3530-3541.

Radhakrishna, H. and Donaldson, J. G. (1997). ADP-ribosylation factor 6 regulates a novel plasma membrane recycling pathway. *J. Cell Biol.* **139**, 49-61.

Radhakrishna, H., Al-Awar, O., Khachikian, Z. and Donaldson, J. G. (1999). ARF6 requirement for Rac ruffling suggests a role for membrane trafficking in cortical actin rearrangements. *J. Cell Sci.* **112**, 855-866.

Rozelle, A. L., Machesky, L. M., Yamamoto, M., Driessens, M. H., Insall, R. H., Roth, M. G., Luby-Phelps, K., Marriott, G., Hall, A. and Yin, H. L. (2000). Phosphatidylinositol 4,5-bisphosphate induces actin-based movement of raft-enriched vesicles through WASP-Arp2/3. *Curr. Biol.* **10**, 311-320.

Ruppel, K. M. and Spudich, J. A. (1996). Structure-function analysis of the motor domain of myosin. *Annu. Rev. Cell Dev. Biol.* **12**, 543-573.

Ruppert, C., Godel, J., Muller, R. T., Kroschewski, R., Reinhard, J. and Bahler, M. (1995). Localization of the rat myosin I molecules myr 1 and myr 2 and in vivo targeting of their tail domains. *J. Cell Sci.* **108**, 3775-3786.

Saeki, K., Miura, Y., Aki, D., Kurosaki, T. and Yoshimura, A. (2003). The B cell-specific major raft protein, Raftlin, is necessary for the integrity of lipid raft and BCR signal transduction. *EMBO J.* **22**, 3015-3026.

Simons, K. and Toomre, D. (2000). Lipid rafts and signal transduction. *Nat. Rev. Mol. Cell Biol.* **1**, 31-39.

Simons, K. and Gerl, M. J. (2010). Revitalizing membrane rafts: new tools and insights. *Nat. Rev. Mol. Cell Biol.* **11**, 688-699.

Sprenger, R. R., Speijer, D., Back, J. W., De Koster, C. G., Pannekoek, H. and Horrevoets, A. J. (2004). Comparative proteomics of human endothelial cell caveolae and rafts using two-dimensional gel electrophoresis and mass spectrometry. *Electrophoresis* **25**, 156-172.

Steinman, R. M., Mellman, I. S., Muller, W. A. and Cohn, Z. A. (1983). Endocytosis and the recycling of plasma membrane. *J. Cell Biol.* **96**, 1-27.

Tang, N., Lin, T. and Ostap, E. M. (2002). Dynamics of myo1c (myosin-ibeta) lipid binding and dissociation. *J. Biol. Chem.* **277**, 42763-42768.

Tang, N., Lin, T., Yang, J., Foskett, J. K. and Ostap, E. M. (2007). CIB1 and CaBP1 bind to the myo1c regulatory domain. *J. Muscle Res. Cell Motil.* **28**, 285-91.

Tiwari, R. K., Kusari, J. and Sen, G. C. (1987). Functional equivalents of interferon-mediated signals needed for induction of an mRNA can be generated by double-stranded RNA and growth factors. *EMBO J.* **6**, 3373-3378.

Toyoda, T., An, D., Witczak, C. A., Koh, H. J., Hirshman, M. F., Fujii, N. and Goodyear, L. J. (2011). Myo1c regulates glucose uptake in mouse skeletal muscle. *J. Biol. Chem.* **286**, 4133-4140.

Wagner, M. C., Barylko, B. and Albanesi, J. P. (1992). Tissue distribution and subcellular localization of mammalian myosin I. *J. Cell Biol.* **119**, 163-170.

Wagner, M. C., Blazer-Yost, B. L., Boyd-White, J., Srirangam, A., Pennington, J. and Bennett, S. (2005). Expression of the unconventional myosin Myo1c alters sodium transport in M1 collecting duct cells. *Am. J. Physiol. Cell Physiol.* **289**, C120-C129.

Yip, M. F., Ramm, G., Larance, M., Hoehn, K. L., Wagner, M. C., Guilhaus, M. and James, D. E. (2008). CaMKII-mediated phosphorylation of the myosin motor Myo1c is required for insulin-stimulated GLUT4 translocation in adipocytes. *Cell Metab.* **8**, 384-398.

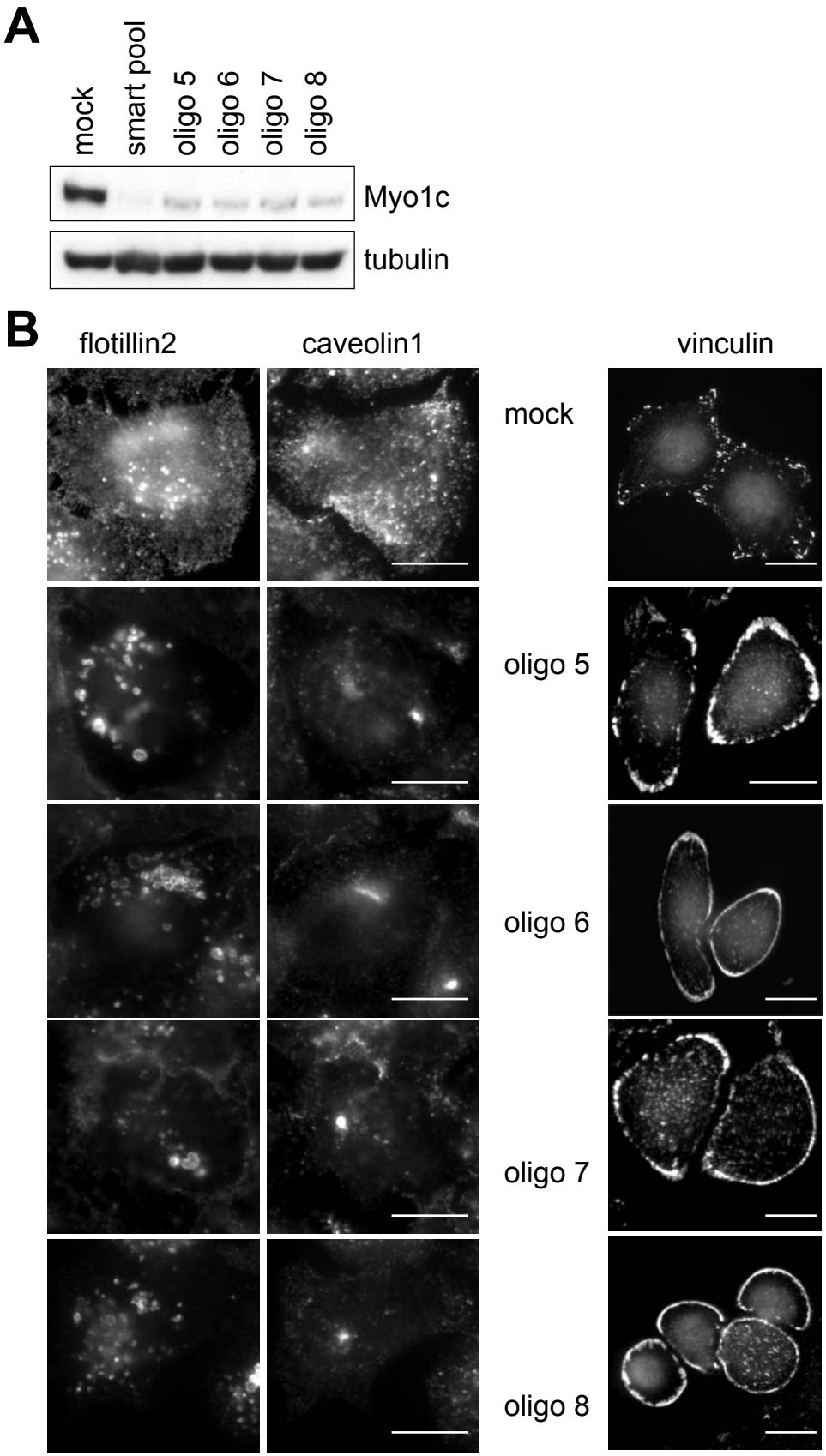

Fig. S1: Single siRNA oligos targeting Myo1c cause redistribution of lipid rafts and focal adhesions. (A) HeLa cells were either mock transfected, transfected with single siRNA oligos specific to Myo1c or with a siRNA smart pool, which combines all four oligos. Cell lysates were blotted and probed with antibodies to Myo1c and α-tubulin as a loading control to confirm the successful Myo1c depletion. **(B)** Mock and Myo1c depleted cells using single oligos were labeled with antibodies to flotillin2, caveolin1 or vinculin. Bars, 10μm

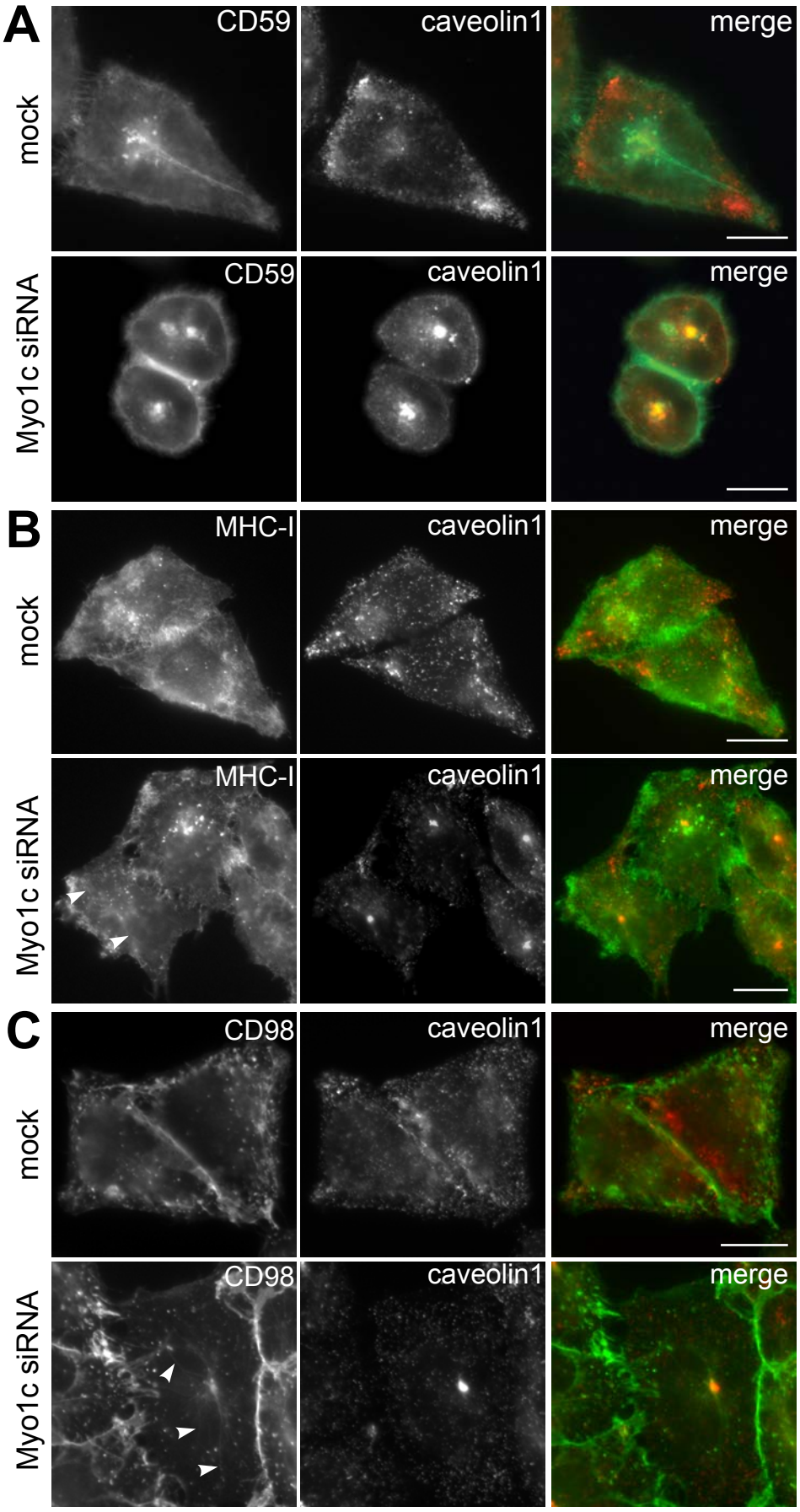

Fig. S2: Depletion of Myo1c redistributes CD59, but does not affect CD98 or MHC-class I localization. (A) HeLa cells were mock treated or treated with siRNA specific to Myo1c and stained with antibodies to caveolin1 and lipid raft marker CD59 for immunofluorescence microscopy. **(B, C)** Mock and Myo1c knockdown cells were incubated in the presence of antibodies to MHC-I **(B)** or CD98 **(C)** for 1 hour at 37°C, then fixed and labelled with anti-caveolin1 antibodies for immunofluorescence microscopy. Bars, 10μm

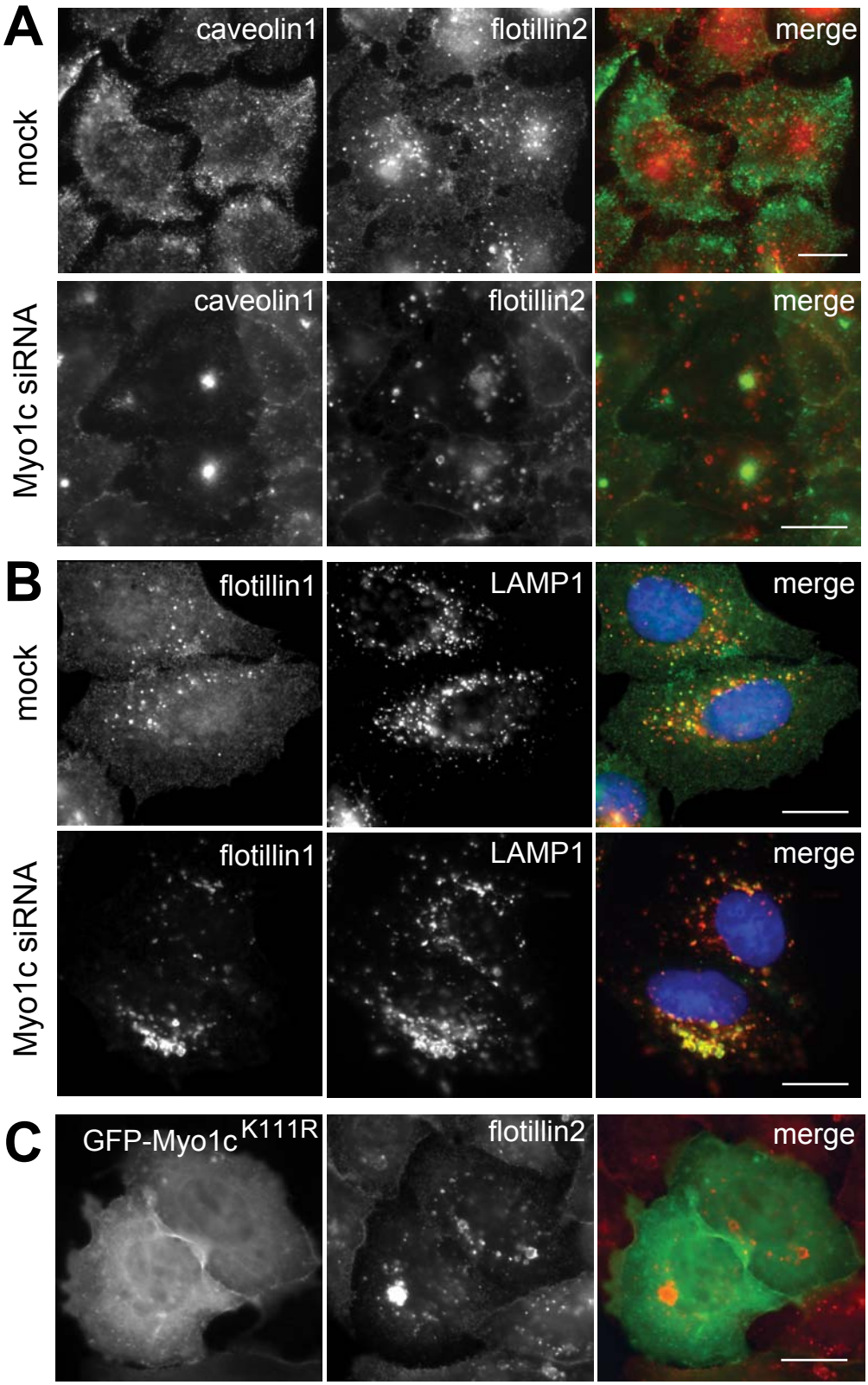

Fig. S3: Depletion of Myo1c redistributes lipid raft markers flotillin1 and 2. (A) HeLa cells were mock treated or treated with siRNA specific to Myo1c and stained with antibodies to caveolin1 and flotillin2 for immunofluorescence microscopy. **(B)** Mock or Myo1c depleted HeLa cells were labeled with antibodies to flotillin1 and the late endosomes/lysosome marker LAMP1 for confocal microscopy. Cell nuclei are shown in blue in the merged images. **(C)** HeLa cells transiently transfected with the dominant negative GFP-Myo1cK111R rigor mutant were labeled with antibodies to GFP and flotillin2. Bars, 10µm

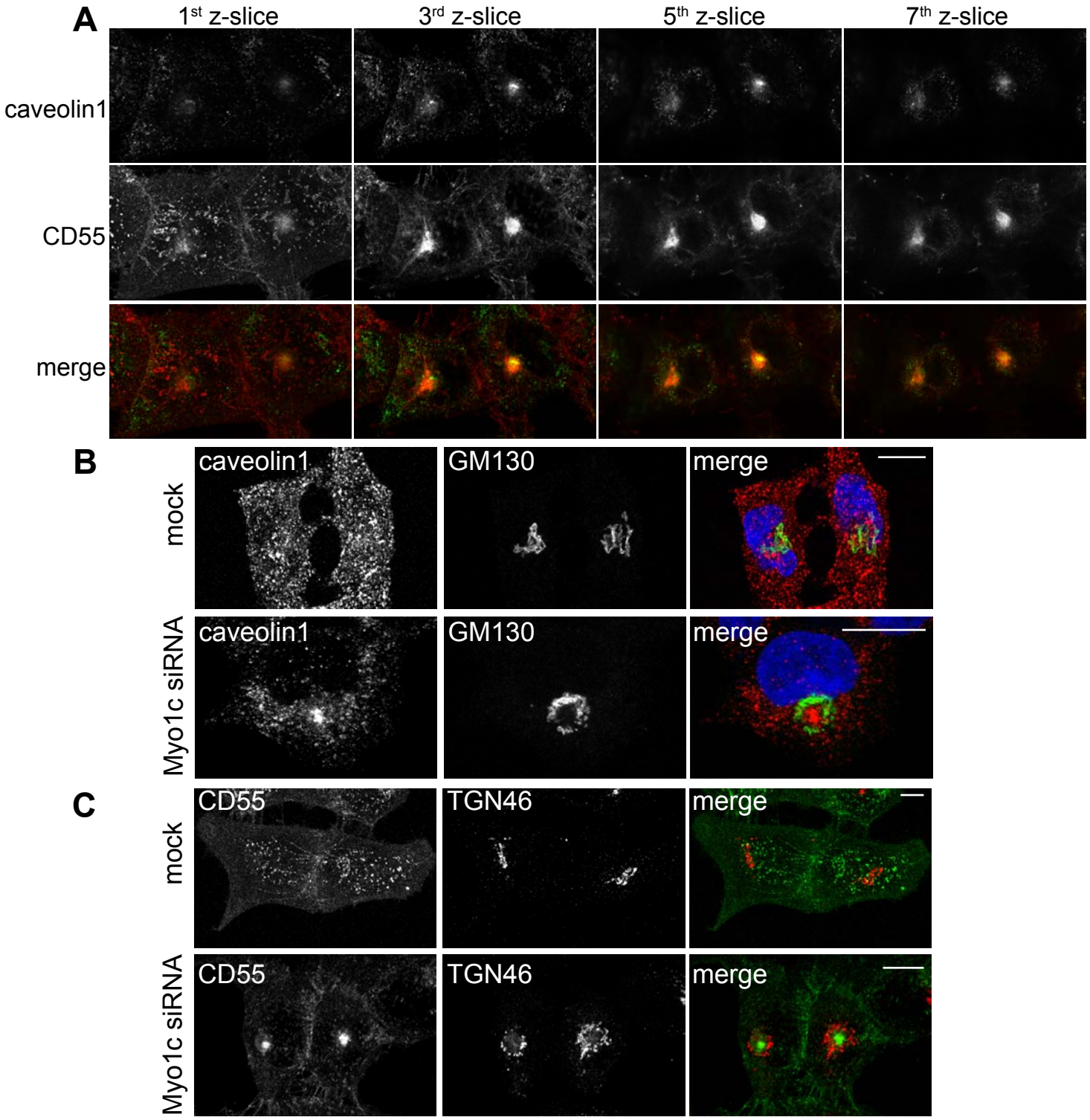

Fig. S4: Depletion of Myo1c causes accumulation of lipid rafts in the peri-nuclear position, which is distinct from the Golgi complex. (A) Myo1c depleted HeLa cells were labelled with anti-CD55 and anti-caveolin1 antibodies and z-stacks were captured using confocal microscopy. Images represent individual optical z-slices (0.33µm thickness). **(B, C)** Mock and Myo1c siRNA treated HeLa cells were stained with antibodies to caveolin1 and the Golgi marker GM130 **(B)** or CD55 and the trans Golgi protein TGN46 **(C)** for confocal microscopy. Images represent a confocal z projection of the whole cell. Bars, 10µm

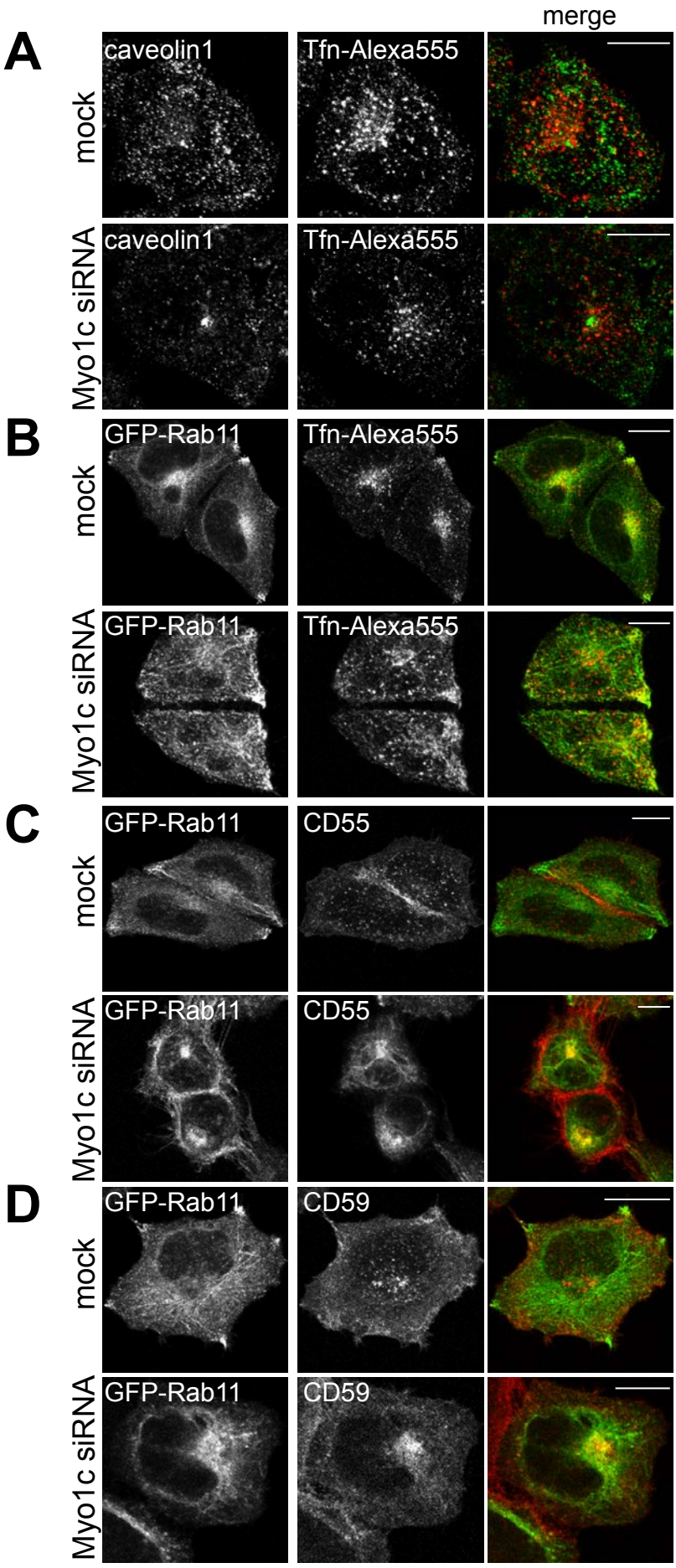

Fig. S5: Depletion of Myo1c does not change the distribution of the transferrin receptor or Rab11. (A) To detect the TfnR along the endocytic/recycling pathway mock or Myo1c depleted HeLa cells were incubated with Tfn-Alexa555 for 1 hour at 37°C, then fixed and labeled with caveolin1 antibodies for confocal microscopy. **(B)** Control and Myo1c knockdown HeLa cells stably expressing GFP-Rab11 were incubated with Tfn-Alexa555 for 1 hour at 37°C, fixed and imaged using a confocal microscope. **(C, D)** To visualize the distribution of lipid rafts in mock and Myo1c siRNA treated HeLa cells stably expressing GFP-Rab11, cells were incubated in the continuous presence of antibodies to CD55 **(C)** or CD59 **(D)** for 1 hour at 37°C, then processed for confocal microscopy. All images represent a confocal z projection of whole cells. Bars, 10μm